

Liver macrophages inhibit the endogenous antioxidant response in obesity-associated insulin resistance

Valerio Azzimato^{1†}, Jennifer Jager^{2†}, Ping Chen^{1†}, Cecilia Morgantini¹, Laura Levi¹, Emelie Barreby¹, André Sulén¹, Carolina Osés¹, Joost Willerbrords¹, Connie Xu¹, Xidan Li¹, Joanne X. Shen³, Naveed Akbar⁴, Lars Haag⁵, Ewa Ellis⁶, Kerstin Wälhen⁷, Erik Näslund⁸, Anders Thorell^{8,9}, Robin P. Choudhury⁴, Volker M. Lauschke³, Mikael Rydén,⁷ Siobhan M. Craige¹⁰, and Myriam Aouadi^{1*}

¹Integrated Cardio Metabolic Center, Department of Medicine, Karolinska Institutet, 141 57 Huddinge, Sweden.

²Université Côte d’Azur, Inserm U1065, C3M, Team Cellular and Molecular Physiopathology of Obesity, 06000 Nice, France.

³Section of Pharmacogenetics, Department of Physiology and Pharmacology, Karolinska Institutet, 171 77 Solna, Sweden

⁴Division of Cardiovascular Medicine, Radcliffe Department of Medicine, University of Oxford, OX3 9DU Oxford, UK.

⁵Department of Laboratory Medicine, Laboratory Medicine, Karolinska Institutet, 141 57 Huddinge, Sweden.

⁶Division of Transplantation Surgery, Clinical Science, Intervention and Technology (CLINTEC), Karolinska Institutet, 141 57 Huddinge, Sweden.

⁷Unit of Endocrinology Department of Medicine, Karolinska Institutet, 141 57 Huddinge, Sweden.

⁸Division of Surgery, Department of Clinical Sciences, Danderyd Hospital, Karolinska Institutet, 182 88 Stockholm, Sweden.

⁹Department of Surgery, Ersta Hospital, Karolinska Institutet, 116 28 Stockholm, Sweden.

¹⁰Human Nutrition, Food, and Exercise Department, Virginia Tech, Blacksburg, VA 24060, USA

*Corresponding Author. e-mail: myriam.aouadi@ki.se

†These authors contributed equally to this study.

One-Sentence Summary: Liver macrophages exacerbate oxidative stress in obesity-induced hepatic steatosis by blocking the endogenous antioxidant response.

Abstract: Obesity and insulin resistance are risk factors for nonalcoholic fatty liver disease (NAFLD), the most common chronic liver disease worldwide. Because no approved medication nor an accurate and non-invasive diagnosis are currently available for NAFLD, there is a clear need to better understand the link between obesity and NAFLD. Lipid accumulation during obesity is known to be associated with oxidative stress and inflammatory activation of liver macrophages (LMs). However, we show that although LMs do not become pro-inflammatory during obesity, they display signs of oxidative stress. In livers of both humans and mice, antioxidant nuclear factor erythroid 2–related factor 2 (NRF2) was downregulated with obesity and insulin resistance, yielding an impaired response to lipid accumulation. At the molecular level, a microRNA targeting NRF2 protein, *miR-144*, was elevated in the livers of obese insulin-resistant humans and mice, and specific silencing of *miR-144* in LMs was sufficient to restore NRF2 protein levels and the antioxidant response. These results highlight the pathological role of LMs and their therapeutic potential to restore the impaired endogenous antioxidant response in obesity-associated NAFLD.

Introduction

Obesity represents a major health issue worldwide as it strongly increases the risk for several metabolic complications including non-alcoholic fatty liver disease (NAFLD), insulin resistance, and type 2 diabetes (T2D) (1, 2). Given its major role in the metabolism of nutrients, the liver plays a central role in the control of metabolic homeostasis (3).

Fatty liver is the result of excessive lipid accumulation due to the lower fat storage capacity of adipose tissue in obesity-associated insulin resistance (4). The inability of the liver to handle this overload of fat leads to aberrant lipid peroxidation and excessive production of reactive oxygen species (ROS) and reactive nitrogen species (RNS) (5). ROS and RNS are thought to trigger the phenotypic switch of liver macrophages (LMs) from an anti-inflammatory (M2) to a pro-inflammatory activation state (M1), leading to insulin resistance (6). The contribution of LMs to oxidative stress in the liver has been debated and despite several reports of LM activation leading to unbalanced and detrimental ROS production in liver diseases (7), the direct role of LMs in the regulation of oxidative stress during the initial disease state was unknown. Indeed, studies have described macrophages and particularly LMs as the major source of ROS (8), primarily referred to pro-inflammatory activated macrophages (9). However, we recently demonstrated that LMs do not undergo pro-inflammatory activation with obesity or insulin resistance in mice or humans (10). We have also demonstrated that, during obesity, LMs produce non-inflammatory factors able to regulate

insulin sensitivity but nonetheless display signs of oxidative stress. Indeed, transcriptomic profiling showed that several metabolic pathways involved in ROS/RNS production such as the tricarboxylic acid cycle (TCA) cycle and oxidative phosphorylation (OXPHOS) were dysregulated in the LMs of obese compared to control mice (10). We therefore hypothesized that LMs may regulate oxidative stress independently of their inflammatory status in obesity-induced insulin resistance.

Nuclear factor erythroid 2-related factor 2 (NFE2L2/Nrf2), a basic leucine zipper transcription factor, is as a master regulator of redox homeostasis (11). Under normal physiological conditions, NRF2 is targeted for proteasomal degradation through its association with Kelch-like ECH-associated protein-1 (KEAP1). Conversely, upon oxidative stress this complex dissociates and NRF2 translocates to the nucleus where it binds to the antioxidant responsive element (ARE), thereby driving the antioxidant response. The antioxidant capacity of the liver is reduced in obesity, although the molecular mechanisms underlying this impairment remain unknown (12). miRNAs are short, single-stranded non-coding RNAs of approximately 21–23 nucleotides in length (13) which bind to target mRNAs at the 3'UTR region and exerts their function through mRNA degradation or protein translation inhibition (14). We demonstrate that, in mouse models of obesity-induced insulin resistance characterized by excessive hepatic lipid accumulation and in human obese individuals, LMs produce miRNAs that impair the antioxidant capacity of the liver but are not linked to activation of pro-inflammatory pathways.

Results

Oxidative stress in LMs fails to trigger an antioxidant response in obesity-induced insulin resistance

Increased lipid peroxidation products are a common marker of oxidative stress (15). To confirm that high-fat diet (HFD)-induced obesity is associated with increased lipid peroxidation in the liver, we measured concentrations of malondialdehyde (MDA), a reactive aldehyde produced during lipid peroxidation, in livers of obese mice. As expected, mice fed a HFD for 9 weeks showed a significant increase in weight and impaired glucose handling ($P < 0.0001$; fig. S1A-B) coupled with increased hepatic lipid and MDA accumulation ($P < 0.0001$; Fig. 1A-B). In addition, ROS release in media cultured with LMs isolated from obese HFD mice was increased compared to normal diet controls (Fig. 1C). Intracellular RNS concentrations also increased in the isolated LMs (Fig. 1D). Moreover, treatment of obesity-associated LMs with superoxide dismutase (SOD), catalase (CAT), or the inhibitor of nitric oxide synthase (NOS) activity N(ω)-nitro-L-arginine methyl ester (L-NAME)

highlighted that both ROS and RNS contribute to oxidative stress in LMs during obesity (fig. S1C-F).

To study the phenotype of LMs in obesity we analyzed the transcriptomic profiles of obese *ob/ob* mice at two different ages (9 and 14 weeks) compared to age-matched wildtype (wt) lean controls. Gene ontology (GO) enrichment analysis revealed oxidative stress as one of the most dysregulated biological processes in obesity (Fig. 1D, table S1 and table S2 in data file S1). In addition, pathway analysis demonstrated impairment of lipid oxidation and antioxidant response pathways in obese compared with lean mice (Fig. 1E, complete list in table S3 and table S4). We observed dsimilar findings in the LMs of mice fed a HFD for 9 weeks, where pathways involved in oxidative stress were enriched compared to normal diet controls (fig. S1G-H, table S5 and table S6). Consistent with our previous findings (10), transcriptomic profiling failed to reveal a proinflammatory phenotypic switch in liver macrophages in obese compared to ND mice (fig. S1I, tables S7 and table S8).

Because oxidative stress is known to trigger the endogenous antioxidant response under the control of the transcription factor *NRF2*, we measured *NRF2* expression in LMs from *ob/ob* mice. We observed that mRNA expression of *Nrf2* was not changed in LMs of obese mice compared to lean mice (Fig. 1F). As RNA-seq only measures steady-state transcript abundance, we also performed global run-on sequencing (GRO-seq) which allows the measurement of nascent transcripts. This revealed that *Nrf2* transcription remained unchanged in HFD mice (Fig. 1G). RNA-seq and GRO-seq analysis indicated that expression of most NRF2 target genes remained unchanged in obesity despite the increased ROS in LMs (Fig. 1H-I, table S9). However, we observed a decrease in NRF2 protein expression in the LMs of HFD-fed mice compared to controls (Fig. 1J). NRF2 was also decreased in hepatocytes and whole livers of HFD-fed mice compared to ND controls (Fig. 1K-L) and in livers of *ob/ob* mice compared to wt (Fig. 1L). Therefore, the antioxidant response driven by NRF2 is impaired in LMs and hepatocytes in both HFD- and genetically induced obesity.

To test whether the impaired antioxidant response observed in livers from obese mice also occurred in humans we measured oxidative stress and *NRF2* mRNA and protein in lean, obese insulin-sensitive, and obese insulin-resistant individuals (Table 1). We observed increased lipid peroxidation and significantly higher intracellular ROS and RNS accumulation in the livers of obese compared to lean individuals (fig. S1J). These ROS and RNS were exacerbated in insulin resistance and associated with liver oxidative stress, obesity, and insulin resistance ($P < 0.001$, $P < 0.01$, $P < 0.05$; Fig. 1M). As in mice, we observed no change in human *NRF2* mRNA (Fig. 1N), but NRF2 protein expression was greatly decreased in obese insulin-resistant individuals compared to obese insulin-sensitive or lean individuals (Fig. 1O). Taken together, these results demonstrate that oxidative stress

fails to induce an NRF2-mediated antioxidant response during obesity-associated insulin resistance in mouse and human livers.

Fig.1

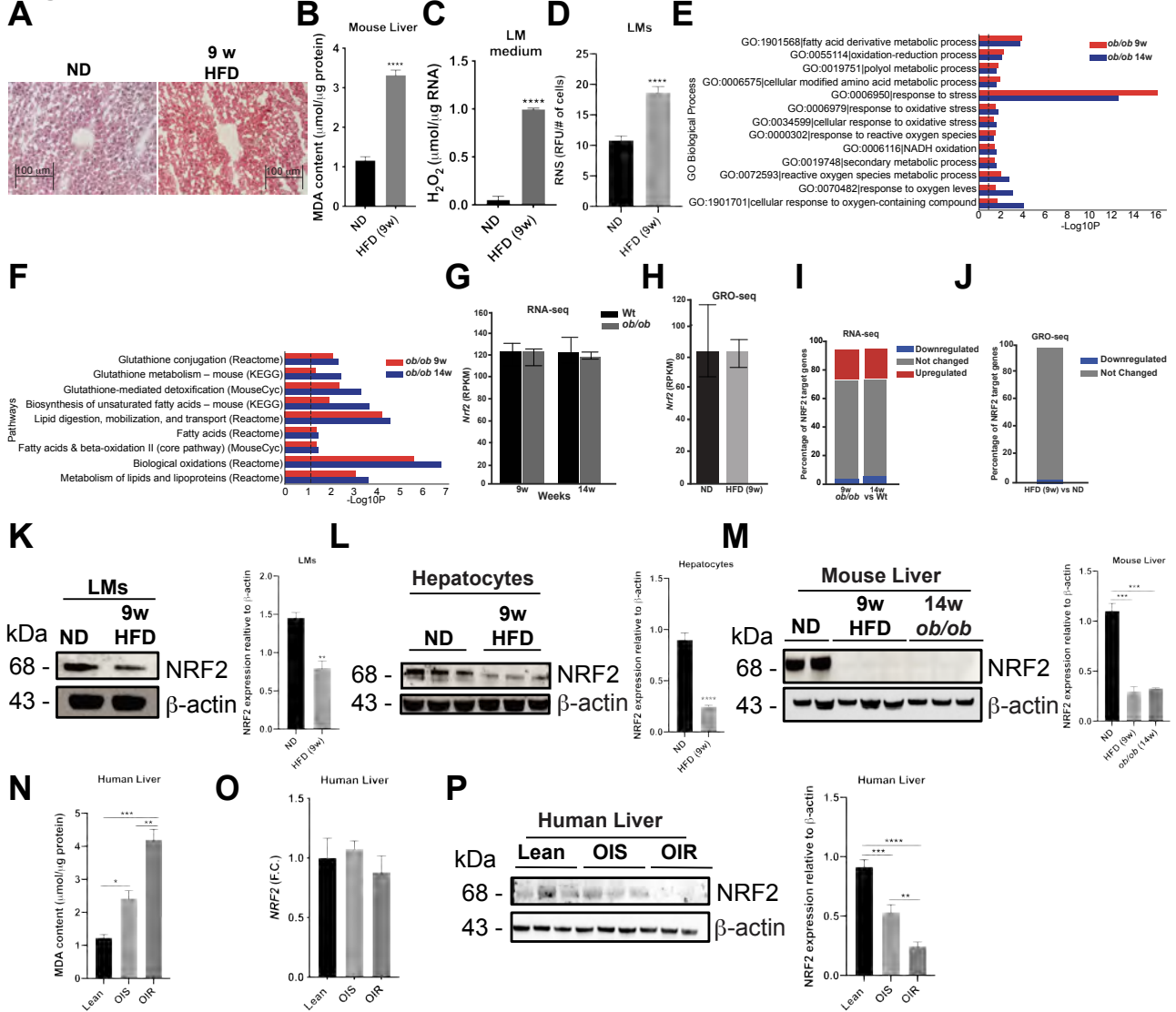


Fig. 1: Oxidative stress in LMs fails to trigger an antioxidant response in obesity-induced insulin resistance. (A-B) Liver Oil-Red-O staining (A) and MDA content (B) of mice fed a HFD or ND for 9 weeks (scale bars, 100 μ m; n=4 per group). **(C)** Extracellular H_2O_2 content in media from LMs of mice fed a HFD or ND for 9 weeks (n=4 per condition). **(D)** Intracellular RNS content in LMs of mice fed a HFD or ND for 9 weeks (n=3 per condition). **(E-F)** Selected significantly enriched Gene Ontology (GO) biological process terms (E) and enriched pathways (F) from genes differentially expressed in LMs of 9- and 14-week-old *ob/ob* mice compared to wt (n=4 wt, n=3 *ob/ob* for 9 weeks; n=4 for 14 weeks). **(G-H)** *Nrf2* expression data from (G) RNA-seq of 9- and 14-week-old wt and *ob/ob* mice and (H) GRO-seq of mice fed a HFD or ND for 9 weeks (n=4 wt, n=3 *ob/ob*,

ND, HFD for 9 weeks; n=4 for 14 weeks). **(I-J)** Percentage of *NRF2* target genes significantly up-regulated, down-regulated or without differential expression in (I) RNA-seq of 9- and 14-week old *ob/ob* mice compared to age-matched wt mice and (J) GRO-seq of mice fed a HFD or ND for 9 weeks (n=4 wt, ND, HFD, n=3 *ob/ob* for 9 weeks; n=4 for 14 weeks. Significance $P < 0.05$. CutOff $0.2 < \log_2 \text{FoldChange} < 0.2$). **(K-M)** Western blots for NRF2 in LMs (K), hepatocytes (L) and whole livers (M) from 9 week- and 14-week-old *ob/ob* mice fed a HFD or ND for (n=3 per condition). **(N)** Liver MDA content from lean, OIS, and OIR human individuals (n=5 per condition). **(O)** RT-qPCR analysis of *Nrf2* in livers from lean, OIS and OIR human individuals (n=5 per condition). Fold change (F.C.) calculation compared to lean. **(P)** Western blots of NRF2 in livers from lean, obese insulin-sensitive (OIS) and obese insulin-resistant (OIR) human individuals (n=5 per condition). Data are mean \pm SEM. ** $p < 0.01$, *** $p < 0.001$, **** $p < 0.0001$. RPKM, reads per kilobase of transcript, per million mapped reads.

NRF2 is a target of *miR-144* in obesity-associated LMs

We next investigated the mechanism(s) whereby NRF2 protein abundance decreased with insulin resistance. Because transcription of *NRF2* is unaffected by obesity and KEAP1 is an important regulator of NRF2 through its ubiquitination and degradation via the proteasome (16), we investigated the KEAP1-NRF2 interaction in livers from obese insulin-resistant, obese insulin-sensitive and lean individuals. Although expression of KEAP1 was unaltered in livers from obese insulin-resistant and insulin-sensitive individuals, the amount of NRF2 associated with KEAP1 was reduced in obesity-associated insulin resistance (Fig. 2A). However, this result could potentially be due to the overall downregulation of NRF2 rather than a decreased interaction between NRF2/KEAP1. Moreover, NRF2 ubiquitination remained unchanged in humans (fig. S2A). These data suggested that the decrease in NRF2 was may be due not just to ubiquitination but was also to an alternative post-transcriptional mechanism independent of KEAP1-induced degradation. Given that NRF2 was downregulated in LMs of obese mice, we analyzed the LM miRNome in diet-induced obese mice to investigate whether miRNAs could regulate NRF2 post-transcriptionally. We performed small-RNA sequencing on LMs of 9 and 14 week-old *ob/ob* mice and found six miRNAs were significantly and commonly upregulated in the obese mice compared to age-matched wt controls ($P < 0.05$; Fig. 2B-C). Using a predictive *in silico* database (17), we noted that *NRF2* was an experimentally validated target of *miR-144*, one of the upregulated miRNAs.

We therefore performed stem-loop RT-qPCR analysis on LMs from both the HFD and *ob/ob* obesity models. We found that *miR-144* expression increased in LMs isolated from HFD mice (Fig. 2D) as

well as in livers of both HFD-fed and *ob/ob* mice compared to their respective controls (Fig. 2E). The observed increase of *miR-144* was liver-specific as its expression remained unchanged in the spleen, lung, and visceral adipose tissue of mice fed a HFD (fig. S2B-D). Furthermore, *miR-144* expression was significantly increased in livers of obese insulin-resistant compared to obese insulin-sensitive or lean individuals ($P < 0.01$, $P < 0.0001$, $P < 0.001$, respectively; Fig. 2F). Altogether, these data suggest that *miR-144* may mediate the decrease in NRF2 in obesity-associated insulin resistance in both murine and human livers.

Fig.2

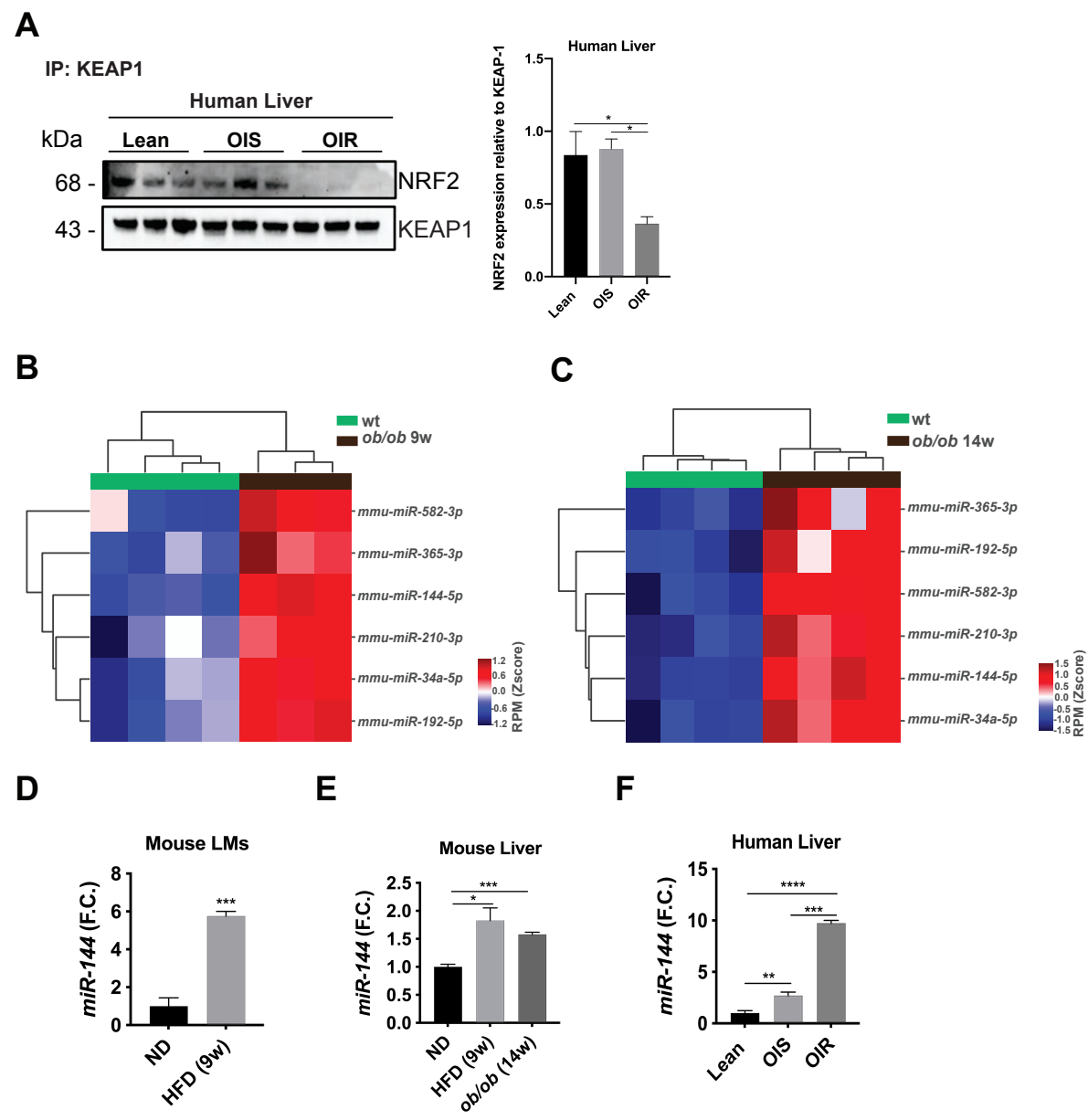


Fig. 2: NRF2 is a target of *miR-144* in obesity-associated LMs. (A) Western blot of NRF2 and KEAP1 after immunoprecipitation of KEAP1 in livers from obese insulin-sensitive (OIS), and obese

insulin-resistant (OIR), and lean human individuals (n=3 per condition). **(B-C)** Heatmaps of significantly (top-down, $P=0.0064$, $P=0.0013$, $P=0.0032$, $P=5.26E-06$, $P=0.0029$, $P=0.0017$) upregulated miRNAs in LMs of 9- (B) and 14- (C) week-old *ob/ob* compared to wt mice (n=4 wt, n=3 *ob/ob* for 9 weeks; n=4 per condition for 14 weeks). **(D-F)** Stem-loop RT-qPCR analysis of *miR-144* in LMs (D) and livers (E) from mice fed a HFD or ND for 9- and 14-week-old *ob/ob* mice (n=3 per condition) and in (F) livers from lean, obese insulin-sensitive (OIS) and obese insulin-resistant (OIR) human individuals (n=5 per condition). Data are mean \pm SEM. RT-qPCR data are fold change (F.C.) compared to ND mice or lean individuals. * $p<0.05$, ** $p<0.01$, *** $p<0.001$, **** $p<0.0001$. RPM, reads per million.

The transcription factor *GATA4* drives the expression of *miR-144* in the liver of insulin-resistant patients

To investigate the mechanism triggering the increase of *miR-144* in insulin resistance, we performed targeted *in silico* analysis of the *miR-144* promoter region. We identified a high density of *GATA4* binding domains on the *miR-144* promoter and enhancer regions (Fig. 3A) which prompted us to analyze whether the expression or phosphorylation of the GATA4 isoform were altered in insulin resistance. In liver protein lysates from obese insulin-resistant subjects, both GATA4 protein expression and phosphorylation were significantly higher than in lysates from obese insulin-sensitive and lean individuals ($P<0.05$, $P<0.01$ respectively; Fig. 3B). To test the hypothesis that *GATA4* induces the expression of *miR-144* in insulin resistance, we performed chromatin immunoprecipitation (ChIP) to analyze specific binding of GATA4 to the *miR-144* promoter region. ChIP analysis confirmed GATA4 increased binding to the *miR-144* promoter in obese insulin-resistant compared to lean individuals (Fig. 3C). We also observed greater amounts in trimethylation of lysine 4 of the histone 3 (H3K4me3) modification, a well-known marker for active transcription, in the insulin-resistant condition (Fig. 3D), suggesting transcription of the *miR-144* locus.

Because oxidative stress is known to activate the *ERK* pathway and lead to the activation of GATA4 by phosphorylation (18), we measured ERK1/2 activity in livers from our human cohort. We observed that ERK1/2 phosphorylation increased with obesity but to similar degrees as in insulin-resistant and insulin-sensitive individuals (Fig. 3E).

We then used the *ob/ob-Erk1^{-/-}* mouse model (19) to validate the role of the *ERK* pathway in the regulation of GATA4 activity in obesity. Western blot analysis showed a decrease of phosphorylated-GATA4 in *ob/ob-Erk1^{-/-}* compared to *ob/ob* and *ob/+* insulin-sensitive control mice (Fig. 3F). *miR-144* was also consistently decreased in livers of *ob/ob-Erk1^{-/-}* mice and in *ob/+* insulin-sensitive mice (Fig. 3G), leading to increased expression of NRF2 and its target genes (Fig. 3H-I).

These data strongly suggested that *miR-144* expression is controlled by GATA4, which is activated by ERK in insulin-resistant mice and humans.

Fig.3

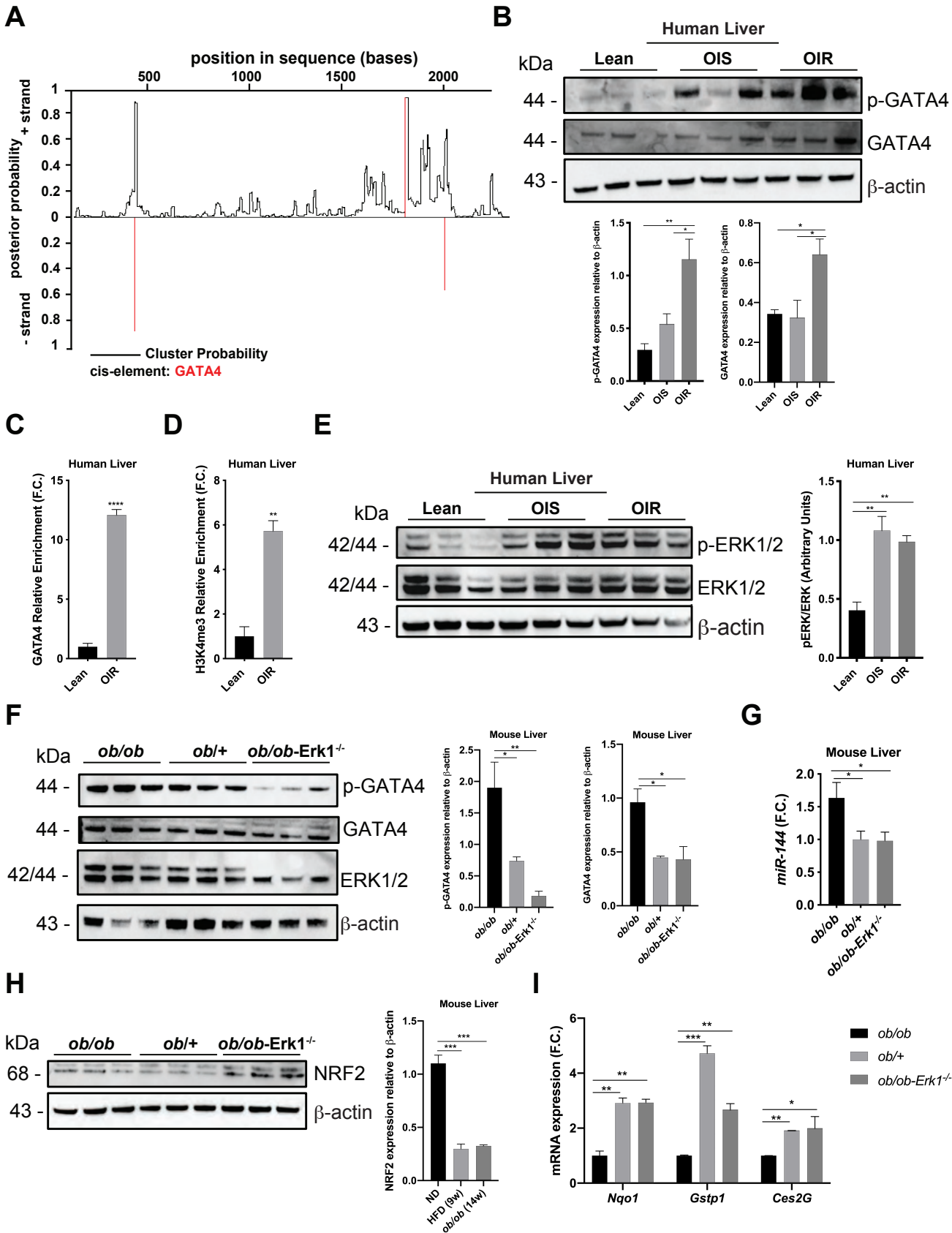


Fig. 3: The transcription factor GATA4 drives the expression of *mir-144* in the liver of insulin-resistant individuals. (A) *In silico* prediction of GATA4-binding domains on the *miR-144* promoter region. (B) Western blots showing phosphorylated-GATA4 and GATA4 in livers from lean, obese insulin-sensitive (OIS), and obese insulin-resistant (OIR) human individuals (n=3 per condition). (C-D) ChIP-qPCR of GATA4 and H3K4me3 relative enrichment on the *miR-144* promoter in livers from lean and OIR human individuals (n=3 per condition). Data are normalized by IgG and fold change (F.C.) compared to lean subjects. (E) Western blots showing phosphorylated-ERK1/2 and ERK1/2 in livers from lean, OIS, and OIR human individuals (n=3 per condition). Quantification of p-ERK1/2/ERK1/2 ratio. (F) Western blots of p-GATA4, GATA4 and ERK1/2 in livers from *ob/+*, *ob/ob*, and *ob/ob-Erk1^{-/-}* mice (n=7 per condition). (G) Stem-loop RT-qPCR analysis of *miR-144* in livers from *ob/+*, *ob/ob*, and *ob/ob-Erk1^{-/-}* mice (n=7 per condition). (H) NRF2 in livers from *ob/+*, *ob/ob*, and *ob/ob-Erk1^{-/-}* mice (n=3 per condition). (I) RT-qPCR analysis of Nrf2 target genes *Nqo1*, *Gstp1* and *Ces2G* in livers from *ob/+*, *ob/ob*, and *ob/ob-Erk1^{-/-}* mice (n=3 per condition). RT-qPCR data are fold change (F.C.) compared to *ob/+*. Data are mean \pm SEM. *p<0.05, **p < 0.01, **** p < 0.0001.

Silencing *miR-144* in LMs reduces ROS release and leads to decreased expression of *miR-144* in hepatocytes

To investigate the role of *miR-144* in the regulation of NRF2 *in vivo*, we used Glucan encapsulated RNAi Particle (GeRP) technology (20, 21) to deliver gene-silencing siRNA specifically in LMs without affecting gene expression in other cells of the liver or the rest of the body. Mice were fed a HFD for 7 weeks and then treated with GeRPs containing an antagomiR targeting *miR-144* (amiR-144) or a non-targeting scrambled control (Fig. 4A). We observed a significant knockdown of *miR-144* as quantified by qPCR in both LMs and hepatocytes isolated from the GeRP-amiR-144-treated mice ($P < 0.05$; Fig. 4B-C). To assess the specificity of GeRP-mediated silencing of *miR-144* we measured the expression of another miRNA, *miR-532*, which remained unchanged upon treatment with GeRP-amiR-144 (Fig. 4D).

We next addressed whether the silencing of *miR-144* observed in hepatocytes following treatment with GeRP-amiR-144 was specific to this particular miRNA or was a general mechanism affecting all miRNAs. We thus treated mice with GeRPs loaded with an antagomir targeting another miRNA, *miR-192*. Treatment with GeRP-amiR-192 significantly decreased *miR-192* expression in LMs but had no effect on hepatocytes ($P < 0.01$; fig. 3SA-B). Furthermore, GeRP-mediated delivery

of a *miR-192* mimic increased *miR-192* expression in LMs but not hepatocytes isolated from the treated mice (fig. 3SC-D). As GeRP-mediated silencing of *miR-144* in hepatocytes seemed specific to this miRNA, we hypothesized that *miR-144* could be delivered from LMs to hepatocytes through extracellular vesicles (EVs). To test whether EV delivery could potentially explain why silencing *miR-144* in LMs led to decreased expression of *miR-144* in hepatocytes, we measured *miR-144* abundance in EVs isolated from the media of LMs collected from mice treated with antagomiR-144. Although control miRNAs *miR-126-3p* and *UNISP6* were present in this media, *miR-144* was undetectable (fig. S3E-I). An alternative explanation for the decreased expression of *miR-144* in hepatocytes following silencing in LMs was a reduction of extracellular ROS which would no longer induce the transcription of *miR-144* in hepatocytes. Thus, we measured the H₂O₂ secreted in the media of murine LMs and hepatocytes after silencing *miR-144* in LMs. Secretion of H₂O₂ was significantly reduced in both LMs and hepatocytes ($P < 0.0001$; Fig. 4E-F), suggesting that silencing of *miR-144* in LMs could alleviate oxidative stress in the liver microenvironment. We then measured the expression and phosphorylation of GATA4 in hepatocytes following the silencing of *miR-144* in LMs isolated from mice. GATA4 phosphorylation was reduced in hepatocytes upon treatment with GeRP-amiR-144 (Fig. 4G), corroborating the notion that silencing *miR-144* in LMs isolated from mice leads to a reduction in *miR-144* transcription in hepatocytes.

To further investigate the regulation of *miR-144* and ROS secretion, we exposed human LMs to different concentrations of H₂O₂ and silenced *miR-144* using antagomir amiR-144 *in vitro*. H₂O₂ treatment increased expression of *GATA4* leading to increased *miR-144* expression which was blunted by amiR-144 (Fig. 4H-J). As expected, H₂O₂ significantly increased the expression of *NRF2* antioxidant target gene *NQO1* ($P < 0.001$), which was further enhanced by silencing *miR-144* ($P < 0.0001$; Fig. 4K). After H₂O₂ treatment, human LMs secreted significantly more H₂O₂, ($P < 0.0001$) which was mitigated by amiR-144 ($P < 0.0001$; Fig. 4L), suggesting a feedback loop between extracellular ROS, intracellular ROS, and *miR-144*/*GATA4* expression.

Using a 3D-culture model of human primary hepatocytes (liver spheroids) (22) we found that treatment with extracellular H₂O₂ was sufficient to induce expression of *miR-144* and *NRF2* target gene *NQO1* (fig. S3J-K). To more closely mimic the *in vivo* liver environment, we added non-parenchymal cells (NPCs) and with free fatty acids (FFAs) to the spheroids to recapitulate the lipid overload in obese livers. Four types of liver spheroids were formed: those with normal *miR-144* expression in both hepatocytes and NPCs, those with *miR-144*-silenced only in NPCs or only in hepatocytes, and those with *miR-144* silenced in both populations (Fig. 4M). As expected, treatment with FFAs boosted *miR-144* expression in liver spheroids (Fig. 4N). Silencing of *miR-144* in the NPCs alone reduced FFA-driven induction of *miR-144* (Fig. 4N), as observed in the mouse model.

Moreover, antagomir-144 administration in hepatocytes alone or in hepatocytes and NPCs together decreased *miR-144* in spheroids treated with FFAs (Fig. 4N). *miR-144* silencing increased NRF2 (Fig. 4O) and the expression of *NRF2* antioxidant target gene *NQO1* (Fig. 4P), leading to a significant decrease in the generation of ROS induced by FFA ($P < 0.001$; Fig. 4Q). These results highlight the importance of *miR-144* expressed by LMs and hepatocytes in the regulation of the endogenous antioxidant response. Considering the low percentage of LMs in liver (6-10%) (10), these results support the importance of LMs in the regulation of *miR-144* expression and ROS secretion in the liver during obesity in mice and humans.

Fig.4

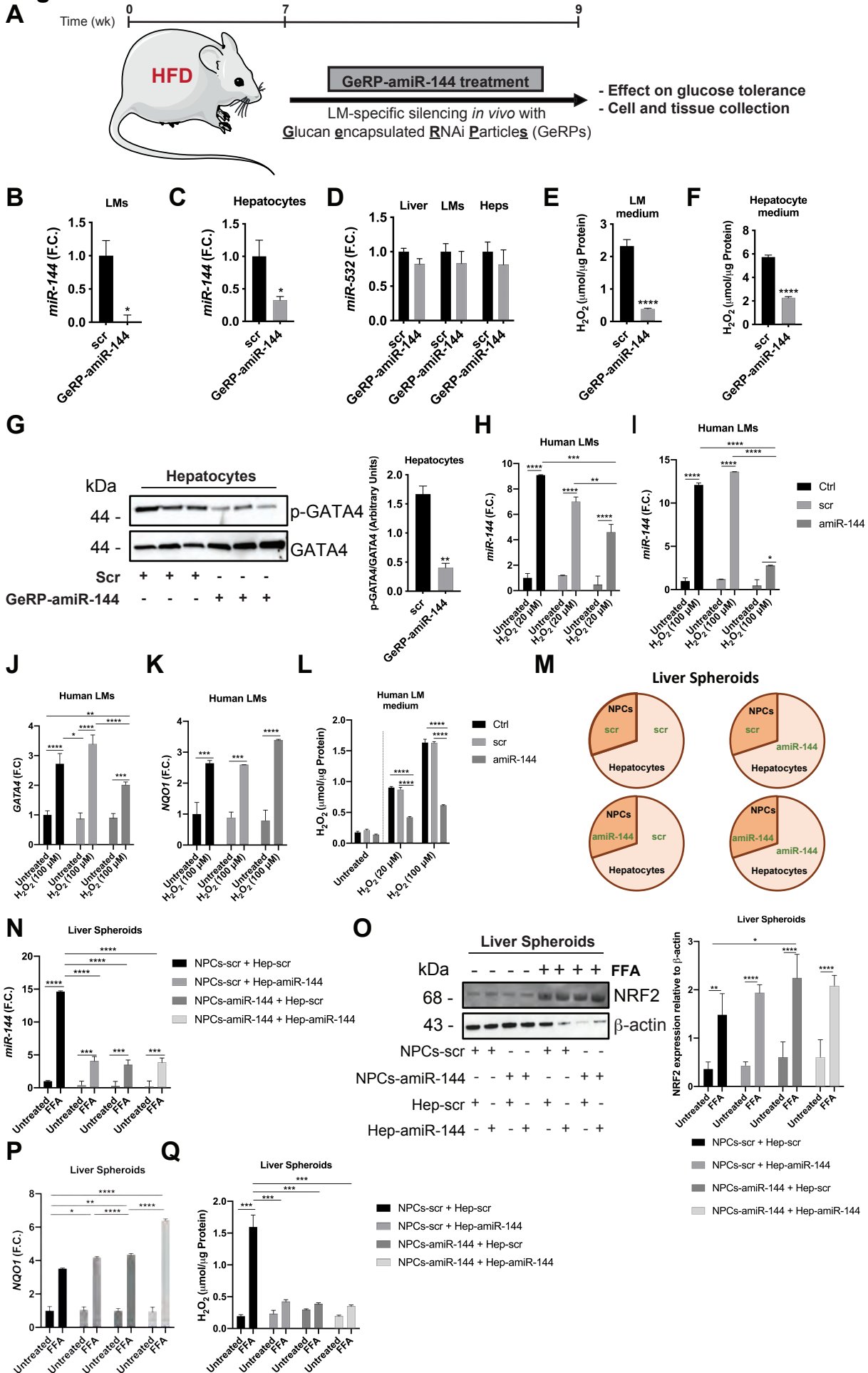


Fig. 4: Silencing *miR-144* in liver macrophages reduces ROS release and leads to decreased expression of *miR-144* in hepatocytes. (A) Protocol of GeRP-amiR-144 treatment. (B-C) Stem-loop RT-qPCR analysis of *miR-144* in LMs (B) and hepatocytes (C) from scrambled control (scr)- and GeRP-amiR-144-treated mice (n=4 per condition). (D) Stem-loop RT-qPCR analysis of *miR-532* in livers, LMs, and hepatocytes from scrambled (scr)- and GeRP-amiR-144-treated mice (n=4 per condition). (E-F) Extracellular H₂O₂ content in media from mice LMs (E) and hepatocytes (F) treated with scr- or GeRP-amiR-144 (n=4 per condition). (G) WB analysis of p-GATA4 and GATA4 in hepatocytes from scr- and GeRP-amiR-144-treated mice (n=3 per condition). Quantification of p-GATA4/GATA4 ratio. (H-I) Stem-loop RT-qPCR analysis of *miR-144* in human LMs untreated, exposed to 20 μ M (H) or 100 μ M (I) H₂O₂ and treated with scr or GeRP-amiR-144 (n=3 per condition). (J-K) RT-qPCR analysis of *GATA4* (J) and *NQO1* (K) in human LMs untreated, exposed to 100 μ M H₂O₂ and treated with scr- or GeRP-amiR-144 (n=3 per condition). (L) Extracellular H₂O₂ content in media from human LMs untreated or exposed to 100 μ M H₂O₂ and treated with scr- or GeRP-amiR-144 (n=3 per condition). (M) Schematic representation of the proportion of liver spheroid cell types and treatments. (N) Stem-loop RT-qPCR of *miR-144* in hepatocytes and NPCs from human liver spheroids exposed to FFA and treated with scrambled control or amiR-144 (pooled liver spheroids from 3 human donor). (O) NRF2 in human liver spheroids exposed to FFA and treated with scrambled control or amiR-144 (pooled liver spheroids from 3 human donors). (P) RT-qPCR analysis of NRF2 target gene *NQO1* in human liver spheroids exposed to FFA and treated with \ amiR-144 or scrambled control (pooled liver spheroids from 3 human donors). (Q) Extracellular H₂O₂ content in media from human liver spheroids exposed to FFA and treated with scrambled control or amiR-144 (pooled liver spheroids from 3 human donors). Data are mean \pm SEM. RT-qPCR data are fold change (F.C.) compared to scr. *p<0.05, **p < 0.01, **** p < 0.0001.

Silencing *miR-144* in LMs reduces oxidative stress and improves hepatic metabolism in insulin resistance in mice

Silencing *miR-144* specifically in LMs reduced the expression of *miR-144* in hepatocytes via reduction of GATA4 phosphorylation. Because GATA4 phosphorylation is triggered by oxidative stress, we hypothesized that *miR-144* silencing in LMs could reduce oxidative stress in the obese liver. We first measured NRF2, ROS, and RNS in livers of obese mice treated with either GeRP-amiR-144 or GeRP-Scr. We observed a significant increase of NRF2 in livers of mice treated with GeRP-amiR-144 in whole livers, LMs, and hepatocytes ($P < 0.05$, $P < 0.001$, $P < 0.0001$ respectively; Fig. 5A-C), along with increased expression of *Nrf2* target genes (*Nqo1*, *Gstp1* and *Ces2G*) (Fig. 5D-

E). Silencing *miR-144* in LMs reduced ROS and, to a lesser extent, RNS in livers of treated mice compared to controls (Fig. 5F-H). This result confirmed the hypothesis that silencing *miR-144* in LMs resulted in reduction of *miR-144* expression in hepatocytes due to a decreased production of both ROS and RNS. To further investigate this mechanism, we used amiR-144 to silence *miR-144* in lean healthy mice that produced physiological concentrations of ROS and RNS. Following treatment with Fluorescein (FITC)-labeled GeRPs, LMs containing GeRPs (CD45⁺/F4/80⁺/Cd11b⁺/FITC⁺), empty LMs (CD45⁺/F4/80⁺/Cd11b⁺/FITC⁻) and empty non-LM NPCs (CD45⁻/FITC⁻) were sorted by flow cytometry, and hepatocytes were isolated. amiR-144 treatment did not influence the percentage of resident or recruited macrophages (Fig. 5I). Moreover, although *miR-144* was successfully silenced in FITC⁺ LMs, we observed no effect on the expression of *miR-144* in any other cell fractions (Fig. 5J-M). These data further confirmed that the reduction in *miR-144* in hepatocytes following silencing in LMs was due to a decreased oxidative stress leading to diminished transcription of *miR-144* via *GATA4*.

We then assessed whether the increase in NRF2 and reduced liver oxidative stress had an effect on whole-body metabolism. We did not observe changes in body weight or total triglyceride content in livers upon treatment with GeRP-amiR-144 (fig. S4A-C). However, transmission electronic microscopy (TEM) revealed an increase in the number of mitochondria following *miR-144* silencing, suggesting an adaptive mechanism to protect hepatocytes against oxidative stress (Fig. 5N-O). Stored intracellular glycogen in the liver was increased in mice treated with GeRP-amiR-144 (Fig. 5P). We thus assessed whether silencing *miR-144* could impact whole body glucose metabolism. Consistent with the increased glycogen stores, glucose tolerance tests showed improved glucose homeostasis in mice treated with GeRP-amiR-144 compared to control mice (Fig. 5Q). This effect was specific for *miR-144* as we did not detect any differences following treatment with GeRP-amiR-192 (fig. S4D). These data suggested that *miR-144* expressed by LMs and hepatocytes contribute to liver oxidative stress and glucose homeostasis in obesity. All together these results demonstrate that *miR-144* decreased NRF2 protein in the liver, resulting in an impaired antioxidant response in obese insulin-resistant mice and humans (fig. S5).

Fig.5

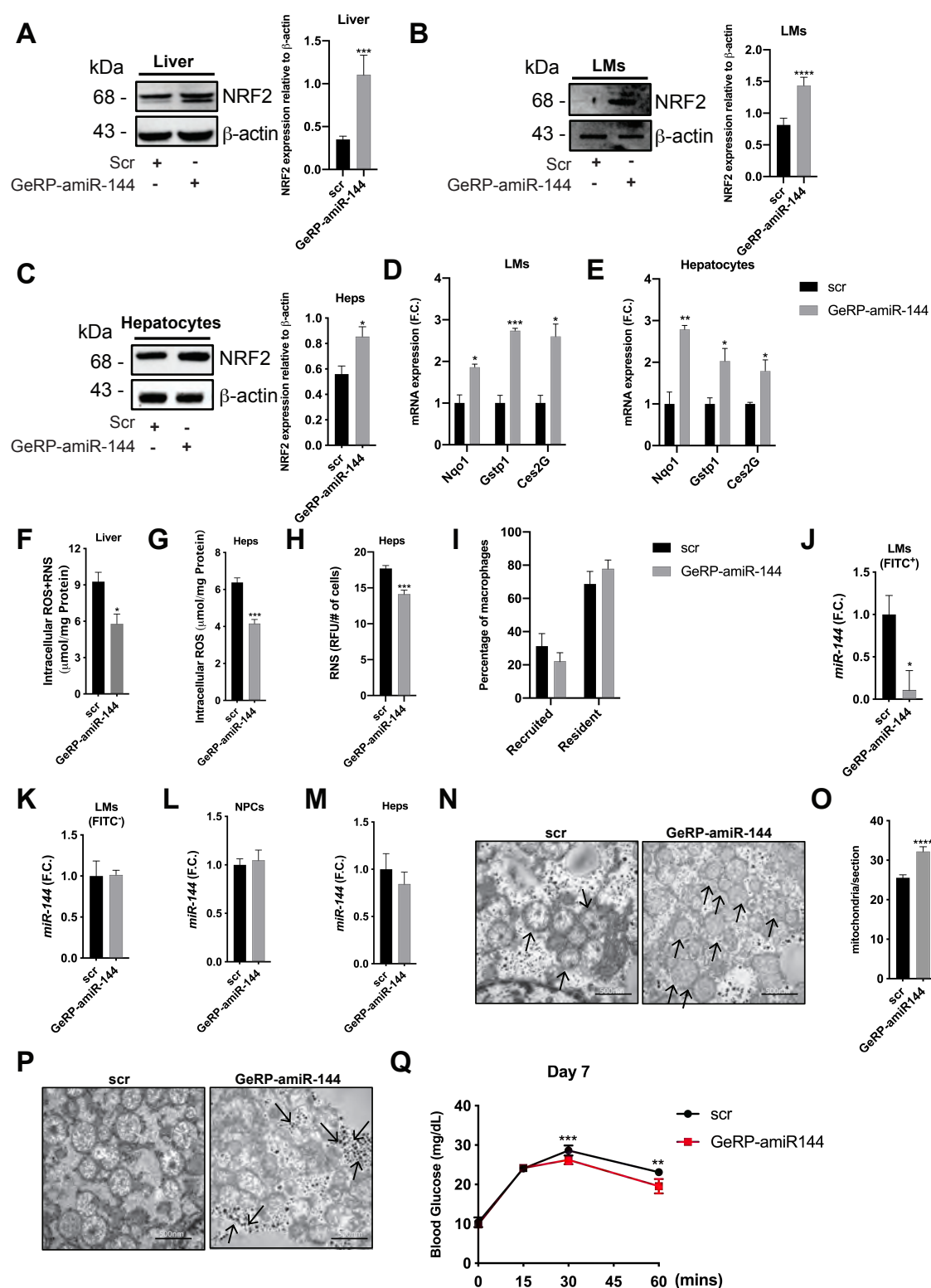


Fig. 5: Silencing *miR-144* in LMs reduces oxidative stress and improves hepatic metabolism in insulin resistance. (A-C) NRF2 in mouse livers (A), LMs (B), and hepatocytes (C) treated with

scrambled control (scr) or GeRP-amiR-144 (n=4 per condition). **(D-E)** RT-qPCR analysis of NRF2 target genes *Nqo1*, *Gstp1*, and *Ces2G* in LMs and hepatocytes from scrambled control- and GeRP-amiR-144-treated mice (n=4 per condition). **(F)** Total intracellular ROS/RNS content in livers from scr - and GeRP-amiR-144-treated mice (n=4 per condition). **(G-H)** Intracellular ROS (G) and RNS (H) in hepatocytes from scr- and GeRP-amiR-144-treated mice (n=4 per condition). **(I)** Percentage of resident and recruited macrophages from scr - and GeRP-amiR-144-treated ND-fed mice (n=4 per condition). **(J-L)** Stem-loop RT-qPCR analysis of *miR-144* in (J) CD45⁺/F4/80⁺/Cd11b⁺/FITC⁺ LMs, (K) CD45⁺/F4/80⁺/Cd11b⁺/FITC⁻ LMs, and (L) CD45⁻/FITC⁻ non-parenchymal cells (NPCs) from scr - and GeRP-amiR-144-treated ND-fed mice (n=4 per condition). **(M)** Stem-loop RT-qPCR analysis of *miR-144* in hepatocytes from scr- and GeRP-amiR-144-treated ND-fed mice (n=4 per condition). **(N)** TEM showing an increased number of mitochondria in livers from scr - and GeRP-amiR-144-treated mice (n=2 per condition). Black arrows depict mitochondria. Scale bars, 500 nm. **(O)** Number of mitochondria per section in livers from scr - and GeRP-amiR-144-treated mice (n=20 sections per condition). **(P)** TEM showing increased stored glycogen in livers from scr - and GeRP-amiR-144 treated mice (n=2 per condition). Black arrows depict glycogen deposits. Scale bars, 500 nm. **(Q)** IP-GTT of scr - and GeRP-amiR-144-treated mice (n=5 per condition). Data are mean \pm SEM. RT-qPCRs data are fold change (F.C.) compared to scr. *p<0.05, **** p < 0.0001.

Discussion

In this study, we investigated the role of LMs in the regulation of the antioxidant response in the livers of obese insulin-resistant humans and mice. Previous studies suggested that oxidative stress and associated damage could represent a link between obesity and liver disease (23 24, 25, 26). We confirmed oxidative stress was triggered by obesity in murine and human livers.

Herein we showed that lipid oxidation and the anti-oxidative response were among the most impaired pathways in two models of obesity.

The main mechanism protecting against oxidative stress, in mice and in humans, is the NRF2/ARE pathway, which induces the expression of antioxidant response genes (27) and directly regulates the homeostasis of both ROS and RNS (28). We found that NRF2 protein expression was reduced in obese mice and human individuals, suggesting an impaired antioxidant response. KEAP1 has been extensively described as the main regulator of NRF2 at the post-transcriptional level. In the absence of oxidative stress, the interaction between NRF2 with KEAP1 facilitates the proteasomal degradation and rapid turnover of NRF2 (27, 28). Conversely, under conditions of oxidative stress, the modification of KEAP1 cysteine residues leads to a change in its conformation that releases

NRF2, which then translocates to the nucleus where it binds to the ARE, subsequently activating the transcription of antioxidant genes (29, 30). Inflammatory activation of macrophages has been associated with a higher production of itaconate from citrate in the TCA cycle which then activates NRF2 through alkylation of KEAP1 (31). In that context, itaconate was described as an anti-inflammatory metabolite able to reduce oxidative stress.

In this study, we found that *Nrf2* mRNA expression remained unchanged upon oxidative stress induced by obesity. Furthermore, neither expression of KEAP1 nor ubiquitination of NRF2 changed during obesity, suggesting a post-transcriptional mechanism regulating NRF2 protein independently of its interaction with KEAP1. Considering that LMs do not undergo inflammatory activation during obesity, the different NRF2 regulation could depend on the type of stimulus and its kinetics. A previous study described a KEAP1-dependent regulation of NRF2 upon inflammatory activation of macrophages by a potent and acute inflammatory stimulus (lipopolysaccharide or IFN- β) (31). However, macrophages in our study were exposed to chronic lipid overload resulting in oxidative stress that did not induce inflammatory activation and may require a more sustainable mechanism of regulation (for example via *miR-144*) than rapid degradation (such as via KEAP1). We also do not exclude the possibility of a differential mechanism of regulation due to the use of different macrophage cell types (blood- and bone-marrow derived macrophages versus liver macrophages). We hypothesized that NRF2 protein could be targeted by a miRNA and thus we analyzed the miRNome of LMs from obese and healthy mice. Among the upregulated miRNAs we detected in obese LMs, *miR-144* has previously been reported to reduce NRF2 protein levels in cancer (32). We found that *miR-144* expression was highly increased in whole livers of obese mice and humans, and insulin resistance was associated with an increase in *miR-144* in humans. To study the mechanism whereby *miR-144* was regulated by insulin resistance, we performed an *in silico* predictive analysis which detected binding sites for the transcription factor GATA4 near the *miR-144* transcriptional start site. ChIP analysis revealed that GATA4 indeed bound the promoter region of *miR-144* to induce its transcription. This is consistent with reports that *miR-144* transcription is regulated by the transcription factor *GATA4* in cardiomyocytes (33). In mice, GATA4 activation via ERK-mediated phosphorylation in cardiomyocytes has been previously shown to be induced by hyperglycemia (18). Our investigations corroborated these findings, as we observed increased ERK phosphorylation in obese patients compared to lean controls. In addition, GATA4 phosphorylation was reduced in livers of obese *Erk1*^{-/-} mice and consequently *miR-144* and NRF2 remained unchanged upon obesity. We note that whereas *miR-144* was increased in insulin-resistant compared to insulin-sensitive obese subjects, ERK1/2 phosphorylation was comparable between the two groups. However, GATA-4 protein expression was higher in obese insulin-resistant individuals, suggesting that the increased

expression of *miR-144* in these individuals might not only be due to the activation of *GATA4* but also to its increased abundance.

Taking advantage of GeRP technology to specifically manipulate gene expression in LMs, we observed a decrease in *miR-144* in LMs and hepatocytes. This result was surprising as GeRPs cannot be delivered to non-phagocytic cells such as hepatocytes (34, 10, 35). We confirmed the specific liver cell distribution of GeRPs by targeting another miRNA, *miR-192*, which was only silenced in LMs and not in hepatocytes. Based on these findings we hypothesized that LMs could deliver *miR-144* to hepatocytes through EVs, and silencing *miR-144* in LMs could therefore result in decreased *miR-144* in both LMs and hepatocytes. However, EVs produced by LMs did not contain *miR-144*, which remained undetectable following silencing of *miR-144*.

The other possible explanation for the concurrent GeRP-driven downregulation of *miR-144* in both LMs and hepatocytes was that silencing *miR-144* in LMs may have reduced ROS and RNS production in the liver and consequently decreased the expression of *miR-144* in hepatocytes. Consistent with this hypothesis, knockdown of *miR-144* in LMs diminished oxidative stress markers in whole livers of obese mice, suggesting crosstalk between LMs and hepatocytes. To test this hypothesis, we focused on H₂O₂ extracellular release from LMs, as H₂O₂ is considered one of the most stable ROS and can cross membranes unlike other ROS (36, 37). Our findings revealed that ROS release by both LMs and hepatocytes decreased following *miR-144* silencing in LMs. However, we found that hepatocytes may also play a role in the regulation of *miR-144*. Silencing *miR-144* in human primary hepatocyte 3D-cultures (22) exposed to H₂O₂ or FFAs was able to efficiently trigger the antioxidant response. ROS and possibly RNS could therefore potentially act as secondary messengers that contribute to a vicious cycle whereby LMs communicate with hepatocytes to increase *miR-144* expression, leading to an impaired antioxidant response. ROS release has been mainly described in pro-inflammatory macrophages (28, 38, 39, 40), whereas we found that ROS production could be dissociated from inflammation in LMs in obesity. In addition, GATA4 phosphorylation was reduced in hepatocytes upon silencing of *miR-144* in LMs, confirming a major role of LMs in the regulation of *miR-144* transcription induced by oxidative stress. Because NRF2 protein was increased upon *miR-144* silencing in LMs, the observed reduction in oxidative stress in these cells could be explained by a restored endogenous antioxidant response. Although additional work will be needed to study the mechanism whereby NRF2 restoration drives the antioxidant response at the subcellular level, the increased number of mitochondria in the livers of mice treated with the antagomiR-144 suggests an effect on mitochondrial biogenesis, as previously described (41, 42).

Last, silencing *miR-144* expression in LMs improved glucose tolerance and increased liver glycogen stores in obese mice. Consistent with a role of ERK1/2 in the activation of GATA4 and subsequent increase in *miR-144*, *ob/ob-Erk1^{-/-}* and obese mice treated with GeRP-amiR-144 shared a similar phenotype (19). Although the molecular mechanism whereby *Erk1* deficiency improved metabolism in *ob/ob* mice is not fully elucidated, our findings suggest that a better antioxidant response might explain the improved liver function in these mice. Indeed, we demonstrated that silencing *miR-144* in human LMs previously treated with H₂O₂ induced the endogenous antioxidant response and reduced *GATA4* expression, suggesting a feedback loop between *GATA4* and *miR-144* transcription in response to ROS.

Although several studies have highlighted the beneficial effects of NRF2 activation (43, 44), long-term NRF2 stimulation has been associated with liver fibrosis (45), reductive stress (46), and promotion of pre-existing malignancies (47). The major advantage of GeRP technology is its ability to manipulate miRNA expression in a transient and specific manner in LMs while leaving other cells and macrophages in the body unaffected. This is particularly important as *in vivo* attempts to reduce oxidative stress using exogenous antioxidants such as vitamin C, vitamin E, or β -carotene have had no beneficial or even deleterious effects (48, 49, 50). The lack of efficacy of these exogenous antioxidants is thought to be due to both non-specific systemic effects and a decrease in the endogenous antioxidant response, highlighting the importance of a targeted approach to increase the endogenous antioxidant response to reduce oxidative stress.

In sum, this study unveils the important role of LMs in the regulation of systemic metabolism in obesity-induced insulin resistance in mice and humans. Specifically, LMs produce miRNAs that impair the antioxidant capacity of the liver in response to excessive lipid accumulation as observed in obesity-associated insulin resistance. We cannot exclude the importance of hepatocytes in the regulation of *miR-144* expression and of the antioxidant response in obesity. However, despite the low percentage of LMs in the liver, we observed a global antioxidant effect of *miR-144*-specific silencing in LMs, highlighting the importance of LMs in the regulation of the endogenous antioxidant response in obesity.

There are limitations to our work. Although silencing *miR-144* led to a systemic effect on glucose metabolism, we did not observe any change in hepatic steatosis and liver TG content. However, our data demonstrated that silencing of *miR-144* affected the cellular response to oxidative stress induced by excess lipid accumulation in liver, rather than lipid deposition itself. Thus, although we do not think that a longer treatment would have an effect on hepatic steatosis, it would be interesting to silence *miR-144* over a longer treatment period than 15 days to address this matter.

Moreover, although our study highlighted the critical crosstalk between LMs and hepatocytes in the upregulation of oxidative stress during obesity, we understand that a better characterization of the specific ROS and RNS populations involved in this process is needed. Indeed, although ROS and RNS share analogies in their production, function and decomposition (51), our results focused on H₂O₂ release, one of the most stable ROS extracellularly (36,37). Because NRF2 regulates both populations (28), we cannot exclude contribution(s) of other ROS or RNS.

Although our study clearly shows that the antioxidant response is impaired in obese insulin-resistant patients and animals through overexpression of *miR-144* targeting NRF2, further work will be required to validate the role of *miR-144* at different points of liver diseases. NAFLD encompasses a spectrum of disease stages from steatosis to NASH and eventually fibrosis leading to cirrhosis and hepatocarcinoma (HCC). We focused our investigation on the initial step (insulin resistance and steatosis). However, it would be important to analyze the role of *miR-144*, NRF2, and oxidative stress at these various phases of fatty liver diseases to understand the role of *miR-144* in the development of NASH and HCC. Last, although we demonstrated that *miR-144* plays an important role in the regulation of the antioxidant response, our experiments were performed using bulk analyses that do not provide information at the single-cell level. Additional single-cell-based assays such as single-cell RNA sequencing will be required to clearly define whether macrophage subpopulations are predominantly affected by insulin resistance and oxidative stress. Despite these limitations, our study suggests that specific targeting of LMs in order to attenuate the burden of oxidative stress during obesity could represent a therapeutic approach for metabolic diseases, which are often associated with chronic liver diseases.

Materials and Methods

Study design

The objective of this study was to investigate the contribution of liver macrophages to the oxidative stress associated with obesity-induced insulin resistance, in mice and humans. To confirm oxidative stress in liver of obese mice and individuals, we measured the content of reactive oxygen/nitrogen species, lipid content and malonyl-dehaldehyde. To assess the endogenous antioxidant response, we measured the protein levels of its master regulator, NRF2 by western blot. Appropriate surgery, diet and controls were included in the study. To analyse the molecular mechanisms involved in NRF2 post-transcriptional regulation, we performed small RNA-seq on liver macrophages of lean and obese mice and qPCR in liver of mice and humans. We demonstrated that miR-144 targets NRF2 in livers tissues obtained from various mouse and human cohorts. Power analyses were not used to calculate

sample sizes; samples were not excluded, and investigators were not blinded during experiments. Before treatment, mice were weighed and glucose tolerance tests performed. Mice were then assigned to treatment groups to ensure similar average initial body weights and glucose intolerance. About 3 to 5 mice were included in each treatment group as indicated in figure legends, and body weights were continuously monitored weekly throughout the treatment period with GeRPs loaded with control scrambled or antagomiR targeting miR-144. Lean, obese insulin sensitive and obese insulin resistant human individuals were scored according to HOMA-IR. Obese patients were matched for body mass index. We used 5 human liver biopsies per condition. For *in vitro* metabolic studies with spheroids, three independent experiments were performed. Primary data are reported in data file S2.

Human subjects

We obtained liver samples from a total of 15 individuals, including ten obese patients (body mass index (BMI) between 35 and 42 kg/m²) undergoing laparoscopic Roux-en-Y gastric bypass surgery at Danderyd hospital or Ersta hospital in Stockholm, Sweden. We obtained liver cells from five non-obese patients and isolated by the Liver Cell Laboratory at the Unit of Transplantation surgery, Department of Clinical Science, Intervention and Technology (CLINTEC) at Karolinska Institutet, Sweden. None of the participants had any previous history of cardiovascular disease, diabetes, gastrointestinal disease, systemic illness, alcohol abuse, coagulopathy, chronic inflammatory disease, any clinical sign of liver damage, or surgical intervention within six months prior to the study. Patients did not follow any special diet before the surgery. Insulin sensitivity was assessed by homeostatic model assessment (HOMA-IR). Of the obese patients, five patients with HOMA-IR <2 were defined as obese insulin-sensitive and five with HOMA-IR >4 as obese insulin-resistant. Hepatic steatosis index (HIS) was calculated as in (52). The Regional Ethical Committee in Stockholm approved the study and all the subjects gave written informed consent for all procedures prior to their participation. Liver cells from non-obese patients were obtained from liver donors and isolated by the Liver Cell Laboratory at the Unit of Transplantation Surgery, Department of Clinical Science, Intervention and Technology (CLINTEC) at Karolinska Institutet.

Mice and diet

Four-week-old wild-type C57BL/6J (WT) and five-week-old *ob/ob* males were obtained from Charles River Laboratories International, Inc. and maintained on a 12-hour light/dark cycle. Animals were given free access to food and water. C57BL/6J WT mice were fed a high-fat diet (HFD) composed of 60% calories from fat, 20% from carbohydrates, 20% from protein (Research Diets Inc.)

at five weeks of age. Control mice were fed a normal chow diet. All experiments were performed at 9 weeks for HFD mice, or at 9 and 14 weeks for *ob/ob* mice. All procedures were performed in accordance with guidelines approved by the Ethical Committee in Stockholm (Stockholms södra djurförsöksetiska nämnd).

GeRP administration by i.v. injection *in vivo*

GeRPs were prepared as previously described (15). WT mice fed a HFD for 8 weeks were randomized to groups according to their body weight and glucose tolerance. Mice were then treated with 12.5mg/kg GeRPs loaded with miRIDIAN microRNA mmu-miR-144-5p hairpin inhibitor (GeRP-amiR-144) (Dharmacon) or with miRIDIAN microRNA hairpin inhibitor negative control #1 (Dharmacon) (247µg/kg) and Endoportor (2.27mg/kg) as a non-targeting scrambled control. Mice received six doses of fluorescently labeled GeRPs by i.v injection over 15 days.

Metabolic analyses in mice

Glucose tolerance tests (IP-GTTs) were performed on the day of the last GeRP injection after a 6hr fast. A dose of 1g/kg glucose was injected i.p. and blood glucose concentrations were measured using a glucometer at defined time points from the tail vein. The following day mice were sacrificed and tissues were collected for subsequent analyses.

Statistical analysis

Data were analysed using GraphPad Prism Software. Statistical significance of differences among groups was analysed using ANOVA or unpaired two-tailed Student's *t* tests were used to compare the mean values of two groups whenever appropriate. Data were presented as mean ± SEM. *p*-values < 0.05 were considered as statistically significant. Sample sizes for each experiment were calculated based on previous data collection and as described in (53). Although we started every *in vivo* experiment with the same number of animals per group, if any individual animal showed any sign of discomfort or an injection failed, we terminated the study for this particular animal in accordance with our ethical permit.

Supplementary Materials

Materials and Methods

Fig. S1: Oxidative stress in LMs fails to trigger an antioxidant response in obesity-induced insulin resistance.

Fig. S2: NRF2 is a target of *miR-144* in obesity-associated LMs.

Fig. S3: Silencing *miR-144* in liver macrophages reduces ROS release and leads to decreased expression of *miR-144* in hepatocytes.

Fig. S4: Silencing *miR-144* in LMs reduces oxidative stress and improves hepatic metabolism in insulin resistance.

Fig. S5: Model of oxidative stress regulation by LMs in obesity.

The following supplemental tables are available in data file S1:

Table S1. GO biological processes (BP) enriched in genes differentially expressed between 9-week-old *ob/ob* and wt mice based on RNA-seq.

Table S2: GO biological processes (BP) enriched in genes differentially expressed between 14-week-old *ob/ob* and wt mice based on RNA-seq).

Table S3: Over-represented pathways between 9-week-old *ob/ob* and wt mice based on RNA-seq.

Table S4: Over-represented pathways between 14-week-old *ob/ob* and wt mice based on RNA-seq.

Table S5: Enriched GO biological processes (BP) between HFD and ND mice based on GRO-seq.

Table S6: Enriched GO biological processes (BP) between HFD- and ND-fed mice based on RNA-seq.

Table S7: Differentially expressed genes in HFD vs. ND mice (GRO-seq) enriched in inflammatory response GO biological process (GO:0006954).

Table S8: Differentially expressed genes in HFD vs. ND mice (RNA-seq) enriched in inflammatory response GO biological process (GO:0006954).

Table S9: Differential expression status of selected NRF2 target genes in 9-week-old *ob/ob* and wt mice.

Data file S2. Raw data from figures.

References and Notes:

1. C. M. Hales, M. D. Carroll, C. D. Fryar, C. L. Ogden, Prevalence of Obesity Among Adults and Youth: United States, 2015-2016. *NCHS Data Brief*, 1-8 (2017).

2. S. E. Kahn, R. L. Hull, K. M. Utzschneider, Mechanisms linking obesity to insulin resistance and type 2 diabetes. *Nature* **444**, 840-846 (2006).
3. L. P. Bechmann, R. A. Hannivoort, G. Gerken, G. S. Hotamisligil, M. Trauner, A. Canbay, The interaction of hepatic lipid and glucose metabolism in liver diseases. *Journal of Hepatology* **56**, 952-964 (2012).
4. D. H. Ipsen, J. Lykkesfeldt, P. Tveden-Nyborg, Molecular mechanisms of hepatic lipid accumulation in non-alcoholic fatty liver disease. *Cell Mol Life Sci* **75**, 3313-3327 (2018).
5. Q. Liu, S. Bengmark, S. Qu, The role of hepatic fat accumulation in pathogenesis of non-alcoholic fatty liver disease (NAFLD). *Lipids Health Dis* **9**, 42 (2010).
6. J. Jager, M. Aparicio-Vergara, M. Aouadi, Liver innate immune cells and insulin resistance: the multiple facets of Kupffer cells. *J Intern Med* **280**, 209-220 (2016).
7. H. Y. Tan, N. Wang, S. Li, M. Hong, X. Wang, Y. Feng, The Reactive Oxygen Species in Macrophage Polarization: Reflecting Its Dual Role in Progression and Treatment of Human Diseases. *Oxid Med Cell Longev* **2016**, 2795090.
8. O. A. Castaneda, S. C. Lee, C. T. Ho, T. C. Huang, Macrophages in oxidative stress and models to evaluate the antioxidant function of dietary natural compounds. *J Food Drug Anal* **25**, 111-118 (2017).
9. L. Formentini, F. Santacatterina, C. Nunez de Arenas, K. Stamatakis, D. Lopez-Martinez, A. Logan, M. Fresno, R. Smits, M. P. Murphy, J. M. Cuezva, Mitochondrial ROS Production Protects the Intestine from Inflammation through Functional M2 Macrophage Polarization. *Cell Rep* **19**, 1202-1213 (2017).
10. C. Morgantini, J. Jager, X. Li, L. Levi, V. Azzimato, A. Sulen, E. Barreby, C. Xu, M. Tencerova, E. Näslund, Liver macrophages regulate systemic metabolism through non-inflammatory factors. *Nature Metabolism* **1**, 445 (2019)
11. S. Vomund, A. Schafer, M. J. Parnham, B. Brune, A. von Knethen, Nrf2, the Master Regulator of Anti-Oxidative Responses. *Int J Mol Sci* **18**, (2017).
12. S. Furukawa, T. Fujita, M. Shimabukuro, M. Iwaki, Y. Yamada, Y. Nakajima, O. Nakayama, M. Makishima, M. Matsuda, I. Shimomura, Increased oxidative stress in obesity and its impact on metabolic syndrome. *J Clin Invest* **114**, 1752-1761 (2004).
13. D. P. Bartel, MicroRNAs: genomics, biogenesis, mechanism, and function. *Cell* **116**, 281-297 (2004).
14. D. P. Bartel, MicroRNAs: target recognition and regulatory functions. *Cell* **136**, 215-233 (2009).

15. F. Ito, Y. Sono, T. Ito, Measurement and Clinical Significance of Lipid Peroxidation as a Biomarker of Oxidative Stress: Oxidative Stress in Diabetes, Atherosclerosis, and Chronic Inflammation. *Antioxidants-Basel* **8**, (2019).
16. K. Itoh, N. Wakabayashi, Y. Katoh, T. Ishii, T. O'Connor, M. Yamamoto, Keap1 regulates both cytoplasmic-nuclear shuttling and degradation of Nrf2 in response to electrophiles. *Genes Cells* **8**, 379-391 (2003).
17. H. Dweep, N. Gretz, miRWalk2.0: a comprehensive atlas of microRNA-target interactions. *Nature Methods* **12**, 697 (2015).
18. P. M. Ku, L. J. Chen, J. R. Liang, K. C. Cheng, Y. X. Li, J. T. Cheng, Molecular role of GATA binding protein 4 (GATA-4) in hyperglycemia-induced reduction of cardiac contractility. *Cardiovasc Diabetol* **10**, 57 (2011).
19. J. Jager, V. Corcelle, T. Gremeaux, K. Laurent, A. Waget, G. Pages, B. Binetruy, Y. Le Marchand-Brustel, R. Burcelin, F. Bost, J. F. Tanti, Deficiency in the extracellular signal-regulated kinase 1 (ERK1) protects leptin-deficient mice from insulin resistance without affecting obesity. *Diabetologia* **54**, 180-189 (2011).
20. M. Aouadi, G. J. Tesz, S. M. Nicoloso, M. Wang, M. Chouinard, E. Soto, G. R. Ostroff, M. P. Czech, Orally delivered siRNA targeting macrophage Map4k4 suppresses systemic inflammation. *Nature* **458**, 1180-1184 (2009).
21. G. J. Tesz, M. Aouadi, M. Prot, S. M. Nicoloso, E. Boutet, S. U. Amano, A. Goller, M. Wang, C. A. Guo, W. E. Salomon, J. V. Virbasius, R. A. Baum, M. J. O'Connor, Jr., E. Soto, G. R. Ostroff, M. P. Czech, Glucan particles for selective delivery of siRNA to phagocytic cells in mice. *Biochem J* **436**, 351-362 (2011).
22. C. C. Bell, V. M. Lauschke, S. U. Vorrink, H. Palmgren, R. Duffin, T. B. Andersson, M. Ingelman-Sundberg, Transcriptional, Functional, and Mechanistic Comparisons of Stem Cell-Derived Hepatocytes, HepaRG Cells, and Three-Dimensional Human Hepatocyte Spheroids as Predictive In Vitro Systems for Drug-Induced Liver Injury. *Drug Metab Dispos* **45**, 419-429 (2017).
23. S. M. Shin, J. H. Yang, S. H. Ki, Role of the Nrf2-ARE pathway in liver diseases. *Oxid Med Cell Longev* **2013**, 763257 (2013).
24. R. F. Schwabe, D. A. Brenner, Mechanisms of Liver Injury. I. TNF-alpha-induced liver injury: role of IKK, JNK, and ROS pathways. *Am J Physiol Gastrointest Liver Physiol* **290**, G583-589 (2006).

25. R. Sano, J. C. Reed, ER stress-induced cell death mechanisms. *Biochim Biophys Acta* **1833**, 3460-3470 (2013).
26. Y. Sumida, E. Niki, Y. Naito, T. Yoshikawa, Involvement of free radicals and oxidative stress in NAFLD/NASH. *Free Radic Res* **47**, 869-880 (2013).
27. W. Tang, Y. F. Jiang, M. Ponnusamy, M. Diallo, Role of Nrf2 in chronic liver disease. *World J Gastroenterol* **20**, 13079-13087 (2014).
28. Q. Ma, Role of Nrf2 in Oxidative Stress and Toxicity. *Annu Rev Pharmacol* **53**, 401-+ (2013)
29. M. McMahon, K. Itoh, M. Yamamoto, J. D. Hayes, Keap1-dependent proteasomal degradation of transcription factor Nrf2 contributes to the negative regulation of antioxidant response element-driven gene expression. *J Biol Chem* **278**, 21592-21600 (2003).
30. T. Nguyen, P. J. Sherratt, C. B. Pickett, Regulatory mechanisms controlling gene expression mediated by the antioxidant response element. *Annu Rev Pharmacol Toxicol* **43**, 233-260 (2003).
31. E. L. Mills, D. G. Ryan, H. A. Prag, D. Dikovskaya, D. Menon, Z. Zaslona, M. P. Jedrychowski, A. S. H. Costa, M. Higgins, E. Hams, J. Szpyt, M. C. Runtsch, M. S. King, J. F. McGouran, R. Fischer, B. M. Kessler, A. F. McGettrick, M. M. Hughes, R. G. Carroll, L. M. Booty, E. V. Knatko, P. J. Meakin, M. L. J. Ashford, L. K. Modis, G. Brunori, D. C. Sevin, P. G. Fallon, S. T. Caldwell, E. R. S. Kunji, E. T. Chouchani, C. Frezza, A. T. Dinkova-Kostova, R. C. Hartley, M. P. Murphy, L. A. O'Neill, Itaconate is an anti-inflammatory metabolite that activates Nrf2 via alkylation of KEAP1. *Nature* **556**, 113-117 (2018).
32. C. Sangokoya, M. J. Telen, J. T. Chi, microRNA miR-144 modulates oxidative stress tolerance and associates with anemia severity in sickle cell disease. *Blood* **116**, 4338-4348 (2010).
33. X. Zhang, X. Wang, H. Zhu, C. Zhu, Y. Wang, W. T. Pu, A. G. Jegga, G. C. Fan, Synergistic effects of the GATA-4-mediated miR-144/451 cluster in protection against simulated ischemia/reperfusion-induced cardiomyocyte death. *J Mol Cell Cardiol* **49**, 841-850 (2010).
34. T. Jourdan, J. K. Park, Z. V. Varga, J. Paloczi, N. J. Coffey, A. Z. Rosenberg, G. Godlewski, R. Cinar, K. Mackie, P. Pacher, G. Kunos, Cannabinoid-1 receptor deletion

- in podocytes mitigates both glomerular and tubular dysfunction in a mouse model of diabetic nephropathy. *Diabetes Obes Metab* **20**, 698-708 (2018).
35. M. Tencerova, M. Aouadi, P. Vangala, S. M. Nicoloso, J. C. Yawe, J. L. Cohen, Y. F. Shen, L. Garcia-Menendez, D. J. Pedersen, K. Gallagher-Dorval, R. A. Perugini, O. T. Gupta, M. P. Czech, Activated Kupffer cells inhibit insulin sensitivity in obese mice. *Faseb Journal* **29**, 2959-2969 (2015).
 36. G. Groeger, C. Quiney, T. G. Cotter, Hydrogen Peroxide as a Cell-Survival Signaling Molecule. *Antioxid Redox Sign* **11**, 2655-2671 (2009).
 37. M. Reth, Hydrogen peroxide as second messenger in lymphocyte activation. *Nat Immunol* **3**, 1129-1134 (2002).
 38. E. McNeill, M. J. Crabtree, N. Sahgal, J. Patel, S. Chuaiphichai, A. J. Iqbal, A. B. Hale, D. R. Greaves, K. M. Channon, Regulation of iNOS function and cellular redox state by macrophage Gch1 reveals specific requirements for tetrahydrobiopterin in NRF2 activation. *Free Radic Biol Med* **79**, 206-216 (2015).
 39. M. Mittal, M. R. Siddiqui, K. Tran, S. P. Reddy, A. B. Malik, Reactive oxygen species in inflammation and tissue injury. *Antioxid Redox Signal* **20**, 1126-1167 (2014).
 40. L. J. Hofseth, S. Saito, S. P. Hussain, M. G. Espey, K. M. Miranda, Y. Araki, C. Jhappan, Y. Higashimoto, P. He, S. P. Linke, M. M. Quezado, I. Zurer, V. Rotter, D. A. Wink, E. Appella, C. C. Harris, Nitric oxide-induced cellular stress and p53 activation in chronic inflammation. *Proc Natl Acad Sci U S A* **100**, 143-148 (2003).
 41. J. Strom, B. Xu, X. Tian, Q. M. Chen, Nrf2 protects mitochondrial decay by oxidative stress. *FASEB J* **30**, 66-80 (2016).
 42. M. Abdalkader, R. Lampinen, K. M. Kanninen, T. M. Malm, J. R. Liddell, Targeting Nrf2 to Suppress Ferroptosis and Mitochondrial Dysfunction in Neurodegeneration. *Front Neurosci* **12**, 466 (2018).
 43. H. Zheng, S. A. Whitman, W. Wu, G. T. Wondrak, P. K. Wong, D. Fang, D. D. Zhang, Therapeutic potential of Nrf2 activators in streptozotocin-induced diabetic nephropathy. *Diabetes* **60**, 3055-3066 (2011).
 44. M. C. Jaramillo, D. D. Zhang, The emerging role of the Nrf2-Keap1 signaling pathway in cancer. *Genes Dev* **27**, 2179-2191 (2013).
 45. H. M. Ni, B. L. Woolbright, J. Williams, B. Copple, W. Cui, J. P. Luyendyk, H. Jaeschke, W. X. Ding, Nrf2 promotes the development of fibrosis and tumorigenesis in mice with defective hepatic autophagy. *J Hepatol* **61**, 617-625 (2014).

46. N. S. Rajasekaran, S. Varadharaj, G. D. Khanderao, C. J. Davidson, S. Kannan, M. A. Firpo, J. L. Zweier, I. J. Benjamin, Sustained activation of nuclear erythroid 2-related factor 2/antioxidant response element signaling promotes reductive stress in the human mutant protein aggregation cardiomyopathy in mice. *Antioxid Redox Signal* **14**, 957-971 (2011).
47. H. Wang, X. Liu, M. Long, Y. Huang, L. Zhang, R. Zhang, Y. Zheng, X. Liao, Y. Wang, Q. Liao, W. Li, Z. Tang, Q. Tong, X. Wang, F. Fang, M. Rojo de la Vega, Q. Ouyang, D. D. Zhang, S. Yu, H. Zheng, NRF2 activation by antioxidant antidiabetic agents accelerates tumor metastasis. *Sci Transl Med* **8**, 334ra351 (2016).
48. I. D. Podmore, H. R. Griffiths, K. E. Herbert, N. Mistry, P. Mistry, J. Lunec, Vitamin C exhibits pro-oxidant properties. *Nature* **392**, 559 (1998).
49. E. R. Miller, 3rd, R. Pastor-Barriuso, D. Dalal, R. A. Riemersma, L. J. Appel, E. Guallar, Meta-analysis: high-dosage vitamin E supplementation may increase all-cause mortality. *Ann Intern Med* **142**, 37-46 (2005).
50. S. M. Lippman, E. A. Klein, P. J. Goodman, M. S. Lucia, I. M. Thompson, L. G. Ford, H. L. Parnes, L. M. Minasian, J. M. Gaziano, J. A. Hartline, J. K. Parsons, J. D. Bearden, 3rd, E. D. Crawford, G. E. Goodman, J. Claudio, E. Winquist, E. D. Cook, D. D. Karp, P. Walther, M. M. Lieber, A. R. Kristal, A. K. Darke, K. B. Arnold, P. A. Ganz, R. M. Santella, D. Albanes, P. R. Taylor, J. L. Probstfield, T. J. Jagpal, J. J. Crowley, F. L. Meyskens, Jr., L. H. Baker, C. A. Coltman, Jr., Effect of selenium and vitamin E on risk of prostate cancer and other cancers: the Selenium and Vitamin E Cancer Prevention Trial (SELECT). *JAMA* **301**, 39-51 (2009).
51. C. C. Winterbourn, Reconciling the chemistry and biology of reactive oxygen species. *Nat Chem Biol* **4**, 278-286 (2008).
52. J. H. Lee, D. Kim, H. J. Kim, C. H. Lee, J. I. Yang, W. Kim, Y. J. Kim, J. H. Yoon, S. H. Cho, M. W. Sung, H. S. Lee, Hepatic steatosis index: a simple screening tool reflecting nonalcoholic fatty liver disease. *Dig Liver Dis* **42**, 503-508 (2010).
53. B. Rosner, *Fundamentals of Biostatistics*. (Belmont, CA: Thomson-Brooks/Cole, 2006).
54. M. Aparicio-Vergara, M. Tencerova, C. Morgantini, E. Barreby, M. Aouadi, Isolation of Kupffer Cells and Hepatocytes from a Single Mouse Liver. *Methods Mol Biol* **1639**, 161-171 (2017).
55. N. Akbar, J. E. Digby, T. J. Cahill, A. N. Tavaré, A. L. Corbin, S. Saluja, S. Dawkins, L. Edgar, N. Rawlings, K. Ziberna, E. McNeill, S. Oxford Acute Myocardial Infarction, E. Johnson, A. A. Aljabali, R. A. Dragovic, M. Rohling, T. G. Belgard, I. A. Udalova, D. R.

- Greaves, K. M. Channon, P. R. Riley, D. C. Anthony, R. P. Choudhury, Endothelium-derived extracellular vesicles promote splenic monocyte mobilization in myocardial infarction. *JCI Insight* **2**, (2017).
56. B. Fang, L. J. Everett, J. Jager, E. Briggs, S. M. Armour, D. Feng, A. Roy, Z. Gerhart-Hines, Z. Sun, M. A. Lazar, Circadian Enhancers Coordinate Multiple Phases of Rhythmic Gene Transcription In Vivo. *Cell* **159**, 1140-1152 (2014).
 57. J. Wijkstrom, M. Gonzalez-Quiroz, M. Hernandez, Z. Trujillo, K. Hultenby, A. Ring, M. Soderberg, A. Aragon, C. G. Elinder, A. Wernerson, Renal Morphology, Clinical Findings, and Progression Rate in Mesoamerican Nephropathy. *Am J Kidney Dis* **69**, 626-636 (2017).
 58. M. C. Frith, U. Hansen, Z. P. Weng, Detection of cis-element clusters in higher eukaryotic DNA. *Bioinformatics* **17**, 878-889 (2001).
 59. D. Kim, G. Pertea, C. Trapnell, H. Pimentel, R. Kelley, S. L. Salzberg, TopHat2: accurate alignment of transcriptomes in the presence of insertions, deletions and gene fusions. *Genome Biol* **14**, R36 (2013).
 60. Y. Liao, G. K. Smyth, W. Shi, featureCounts: an efficient general-purpose program for assigning sequence reads to genomic features. *Bioinformatics* **30**, 923-930 (2014).
 61. R. Quinlan, I. M. Hall, BEDTools: a flexible suite of utilities for comparing genomic features. *Bioinformatics* **26**, 841-842 (2010).
 62. A. Dobin, C. A. Davis, F. Schlesinger, J. Drenkow, C. Zaleski, S. Jha, P. Batut, M. Chaisson, T. R. Gingeras, STAR: ultrafast universal RNA-seq aligner. *Bioinformatics* **29**, 15-21 (2013).
 63. C. Trapnell, B. A. Williams, G. Pertea, A. Mortazavi, G. Kwan, M. J. van Baren, S. L. Salzberg, B. J. Wold, L. Pachter, Transcript assembly and quantification by RNA-Seq reveals unannotated transcripts and isoform switching during cell differentiation. *Nat Biotechnol* **28**, 511-515 (2010).
 64. C. Trapnell, D. G. Hendrickson, M. Sauvageau, L. Goff, J. L. Rinn, L. Pachter, Differential analysis of gene regulation at transcript resolution with RNA-seq. *Nat Biotechnol* **31**, 46-53 (2013).
 65. D. N. Slenter, M. Kutmon, K. Hanspers, A. Riutta, J. Windsor, N. Nunes, J. Melius, E. Cirillo, S. L. Coort, D. Digles, F. Ehrhart, P. Giesbertz, M. Kalafati, M. Martens, R. Miller, K. Nishida, L. Rieswijk, A. Waagmeester, L. M. T. Eijssen, C. T. Evelo, A. R. Pico, E. L. Willighagen, WikiPathways: a multifaceted pathway database bridging metabolomics to other omics research. *Nucleic Acids Res* **46**, D661-D667 (2018).

66. M. Martin. Cutadapt removes adapter sequences from high-throughput sequencing reads. *EMBnet.journal* **17**,(1):10-12 (2011).
67. M. J. Axtell, ShortStack: comprehensive annotation and quantification of small RNA genes. *RNA* **19**, 740-751 (2013).
68. J. Ye, S. McGinnis, T. L. Madden, BLAST: improvements for better sequence analysis. *Nucleic Acids Res* **34**, W6-9 (2006).

Acknowledgments: We are grateful to Robert Harris for his input on the manuscript. **Funding:** This work was supported by research grants from AstraZeneca through the ICMC (M.A.), the Swedish Research council (M.A.: 2015-0358), Stockholm County Council (M.R.), the Novo Nordisk Foundation, including the Tripartite Immunometabolism Consortium (M.A. and M.R. TrIC; NNF15CC0018486), the Strategic Research Program in Diabetes at Karolinska Institutet (M.A. and M.R.), The Erling-Persson Family Foundation (A.T.) and the Diabetes Wellness Foundation Sweden (J.J.). **Author contributions:** V.A., J.J. and P.C. carried out most experiments. C.M L.L., E.B., A.S, J.W., C.O. and C.X. helped with hepatocyte and LM isolation, flow cytometry, and interpretation of the data. J.X.S. and V.M.L. provided and performed liver spheroid treatments. N.A. and R.C. performed extracellular vesicle experiments. L.H. generated all electron microscopy images and measurements. E.E provided biopsies and liver cells from lean individuals. E.N., A.T., E.E., K.W., and M.R. provided human liver biopsies. P.C. and X.L. performed bioinformatics analysis and interpretation. V.A., J.J and M.A. conceived the project, analyzed data, and wrote the manuscript with input from all co-authors. S.M.C. helped with interpretation of the data and contributed to writing the revised manuscript. **Competing interests:** V.A. and M.A. are inventors of a pending filing patent (UK1910299.5) application through Potter Clarkson LLP. V.M.L. is co-founder and shareholder of HepaPredict AB. **Data and materials availability:** All data associated with this study can be found in the paper or supplementary materials. Gene expression data from this study are available from Gene Expression Omnibus database under accession number GSE132801.

Code	Sex	Age	BMI	HOMA-IR	HSI	
6127	M	43	37.2	0.56	46.3	OIS
6006	M	43	40.8	1.1	51	OIS

6108	M	40	39.2	1.56	49.8	OIS
6141	M	54	35.8	1.69	50	OIS
6165	M	42	34.7	1.88	42.5	OIS
6168	M	25	40.3	6.18	53.5	OIR
6157	M	44	36.6	6.99	42.5	OIR
6027	M	38	39.8	10.65	55.6	OIR
5870	M	37	37.7	10.94	45.6	OIR
6029	M	64	39.6	13.28	47.2	OIR

Table 1. Parameters of study individuals. OIS, obese insulin-sensitive; OIR, obese insulin-resistant. Code, specific patient identifier. BMI, body mass index. HOMA, homeostatic model assessment. Insulin sensitivity assessed by HOMA-IR method. HIS: hepatic steatosis index.

Supplementary Materials:

Materials and Methods

Isolation of LMs and hepatocytes from mice

LMs and hepatocytes were isolated as previously described (54). Briefly, livers of anesthetized mice were first perfused with calcium-free Hanks' balanced salt solution (HBSS), followed by collagenase digestion. After digestion the hepatocytes were released by mechanical dissociation of the lobes and underwent several steps of filtration with 94 calcium-containing HBSS and centrifugation at 50g for 3 min. The resulting hepatocyte pellet was washed twice and plated. The supernatant containing non-parenchymal cells was loaded on a Percoll gradient (25% and 50%) and centrifuged for 30 min at 2300 rpm and 4°C. The interphase ring with enriched LMs was collected. The cells were then plated for 30 min and washed twice before RNA or proteins were extracted for subsequent analyses.

Mouse LM antioxidant treatment

Plated LMs were treated with 100 μ M catalase (CAT) (Sigma), 100 μ M superoxide dismutase (SOD) (Sigma) and 100 μ M N ω -Nitro-L-arginine methyl ester hydrochloride (L-NAME) (Sigma) for 2 hours. LMs were then immediately harvested for downstream experiments.

Isolation of LMs from humans

Freshly obtained liver biopsies were cut into small pieces and immediately digested in RPMI media containing collagenase II (0.25 mg/ml, Sigma) and DNase I (0.2 mg/ml, Roche) at 37°C for 30 min. Single cell suspensions were filtered through a cell strainer (75 μ m) and centrifuged at 50g for 3 minutes. The supernatant containing NPCs were loaded on a Percoll gradient and LMs isolated as described above.

Human LM H₂O₂ treatment

Human plated LMs were treated with 20 μ M or 100 μ M H₂O₂ for 30 minutes (followed by maintenance in low glucose/insulin medium for 20 hours) and treated with scr or GeRP-amiR-144 as described above. Cells were harvested after 24 hours and downstream experiments were performed as listed below.

Isolation of RNA, microRNA, real-time quantitative PCR and RNA library preparation

Total RNA and microRNAs extraction and purification was performed using the TRIzol Reagent or the (Thermo Fisher Scientific) or the miRNeasy mini kit (Qiagen) following the manufacturers' protocol. For miRNA analyzes 100ng total RNA were reverse-transcribed and amplified in real-time PCR using miScript-System including miScript RT-Kit (Qiagen), miScript SYBR-Green PCR-Kit and miScript Primer Assay miRBase v12 (Qiagen) according to the manufacturer's protocol. Specific primers for hsa-miR-144 (Qiagen), mmu-miR-144 (Qiagen), mmu-miR-532 (Qiagen) and mmu-miR-192 (Qiagen) were used for stem-loop qPCR. For internal control the expression of the small nuclear RNAs RNU6B (Qiagen) was determined. For real time qPCR, cDNA was synthesized from 0.5µg of total RNA using iScript cDNA Synthesis Kit (Bio-Rad) according to the manufacturer's instructions. Synthesized cDNA forward and reverse primers along with the Sso Advanced Universal SYBR Green Supermix were run on the CFX96 Real-time PCR System (Bio-Rad). 60S acidic ribosomal protein P0 (rplp0) or b-actin were used as reference genes in mice and humans. Primer sequences used for qPCR: mouse *Nrf2* (FW: 5'-CGAGATATACGCAGGAGAGGTAAGA-3'; REV: 5'-GCTCGACAATGTTCTCCAGCTT-3'), mouse *Gata4* (FW: 5'-CCCTACCCAGCCTACATGG-3'; REV: 5'-ACATATCGAGATTGGGGTGTCT-3'), mouse *Nqo1* (FW: 5'-TTCTGTGGCTTCCAGGTCTT-3'; REV: 5'-AGGCTGCTTGGAGCAAAATA-3'), mouse *Gstp1* (FW: 5'-TGTCACCCTCATCTACACCAAC-3'; REV: 5'-CAGGGTCTCAAAGGCTTCAG-3'), mouse *Ces2G* (FW: 5'-TCTCTGAGGTGGTTTACCAAACG-3'; REV: 5'-CCTCTCAGACAGCGCACCAG-3'), mouse β -actin (FW: 5'-TCTACAATGAGCTGCGTGTGG-3'; REV: 5'-GTACATGGCTGGGGTGTGAA-3'), human *NRF2* (FW: 5'-CAGCGACGGAAAGAGTATGA-3'; REV: 5'-TGGGCAACCTGGGAGTAG-3'), human *NQO1* (FW: 5'-GGCAGAAGAGCACTGATCGTA-3'; REV: 5'-TGATGGGA TTGAAGTTCATGGC-3'), human *GSTP1* (FW: 5'-GTAGTTTGCCCAAGGTCAAG-3'; REV: 5'-AGCCACCTGAGGGGTAAG-3'), human *CES2G* (FW: 5'-GTCTTCGCTTGTTGTGTCC-3'; REV: 5'-CGAAGGAGAAAGGCAATGAC-3'), human *GATA4* (FW: 5'-TTCCAGCAACTCCAGCAACG-3'; REV: 5'-GCTGCTGTGCCGTAGTGAG-3'), human *RPLP0* (FW: 5'-CAGATTGGCTACCCAAGTGT-3'; REV: 5'-GGGAAGGTGTAATCCGTCTCC-3'). For ChIP-qPCR following primers were used: hChIPmiR144/451 promoter (FW: 5'-CCTGGGCTGTGCCTGACCAC-3'; REV: 5'-AGCACTGTGAGGGGCTGGGG-3').

For library preparation, RNA integrity was determined using an Agilent Bioanalyzer. Libraries from mouse RNA were prepared using TruSeq Stranded mRNA kit (Illumina). Libraries for small-RNA sequencing were prepared using TruSeq Small RNA kit (Illumina) The concentration of indexed

libraries was quantified by RT-qPCR using the Universal Kapa Library Quantification Kit (KAPA Biosystems). Final libraries were normalized and sequenced on an Illumina HiSeq 3000 sequencer.

Liver spheroids

antagomiR transfections

Cryopreserved primary human hepatocytes (Heps) (Bioreclamation IVT, USA) were mixed with a pre-incubated mixture of Lipofectamine RNAiMAX (Invitrogen) and amiR/inhibitor constructs (1 nmol amiR/inhibitor per 300,000 cells) in OptiMEM (Gibco). In the case of co-culture transfections, cryopreserved hepatocytes and isogenic non-parenchymal cells (NPCs) (Bioreclamation IVT) were transfected separately in suspension with a pre-incubated mixture of Lipofectamine RNAiMAX and amiR/inhibitor constructs (1 nmol amiR/inhibitor per 300,000 cells) in OptiMEM. Cells were transfected for 5 hours with occasional agitation of the suspension. All transfections were performed using low glucose/insulin medium (PAN-Biotech, supplemented with 5.5 mM D-glucose, 0.1 nM insulin, 2 mM L-glutamine, 100 units/mL penicillin, 100 µg/ml streptomycin, 5.5 µg/ml transferrin, 6.7 ng/ml sodium selenite, 100 nM dexamethasone, and 10% FBS).

Spheroid formation

Spheroids were formed from hepatocytes alone or from co-cultures of hepatocytes and NPCs as indicated. In the case of co-cultures, separately-transfected hepatocytes and NPCs were seeded at a ratio of 3:1 (Heps:NPCs). Cells were seeded in ultra-low attachment 96-well plates (Corning) as previously described (22) and were cultured in low glucose/insulin medium. Plates were centrifuged at 180 x g for 2 min. Plates were centrifuged again if cells were not well aggregated. After 6 days, when the spheroids were sufficiently compact, 50 % of the medium was exchanged for serum-free medium.

Free fatty acid supplementation

Free fatty acids were conjugated to 10 % bovine serum albumin (Sigma-Aldrich) at a molar ratio of 1:5 for 2 hours at 40 °C. Spheroids were treated with 240 µM oleic acid (Sigma-Aldrich) and 240 µM palmitic acid (Sigma-Aldrich) in high glucose/insulin medium (Gibco, supplemented with 11.1 mM D-glucose, 1.7 µM insulin, 2 mM L-glutamine, 100 units/mL penicillin, 100 µg/ml streptomycin, 5.5 µg/ml transferrin, 6.7 ng/ml sodium selenite, 100 nM dexamethasone, and 10% FBS) for 5 days. Untreated spheroids were maintained in low glucose/insulin medium. All treatments were performed 8 days after spheroid seeding.

H₂O₂ treatment

Spheroids were treated with 100 μ M H₂O₂ for 30 minutes (followed by maintenance in low glucose/insulin medium for 20 hours). All treatments were performed 8 days after spheroid seeding and in low glucose/insulin medium.

Extracellular vesicle isolation

LMs were isolated as described above and cultured in RPMI (Sigma Aldrich) medium with 10% EV-depleted FBS (ThermoFisher Scientific). Extracellular vesicles (EV) were isolated as previously described (55). Briefly, cell culture media was centrifuged for 10 mins at 300g to pellet cellular debris. Supernatants were combined with phosphate buffered saline (PBS) (ThermoFisher Scientific), transferred to ultracentrifugation tubes (Polyallomer Quick-Seal ultra-clear 16mm \times 76mm tubes, Beckman Coulter) and centrifuged at 120,000g for 2 hours to pellet extracellular vesicles. Isolated extracellular vesicles were resuspended in 100uL PBS and utilized for extracellular vesicles characterization as detailed below.

Extracellular vesicles microRNA analysis

Total RNA and microRNAs isolation and stem loop qPCR were performed on isolated EVs as described above. Specific primers for RNU6B, mmu-miR-126-3p and mmu-miR-144 (QIAGEN) were used for qPCR.

Extracellular vesicle size, concentration and zeta potential

Extracellular vesicles size and concentration was determined by dynamic light scattering using the ZetaView (Particle Metrix, Germany) platform.

Nuclei and library preparation for GRO-seq

GRO-seq was performed as previously described (56), with minor modifications for mouse liver macrophages samples. Nuclei were extracted from liver macrophages (3-4 pooled mice/group) using hypotonic buffer, and visually inspected for quality under a microscope with DAPI staining. The total number of nuclei was determined using a Countess AutomatedCell Counter (Bio-Rad). Nuclear run-on was performed using Br-UTP followed by enrichment with anti-Br-UTP antibodies, reverse transcription and library preparation.

Western blot, immunoprecipitation and chromatin immunoprecipitation assay

30 μ g of proteins were fractionated by SDS-polyacrylamide gel electrophoresis using precast 4-12% gradient gels (ThermoFischer Scientific), transferred to polyvinylidene difluoride membranes

(ThermoFischer Scientific) and probed with a 1:1000 dilution of the primary antibodies indicated below. This was followed by incubation with the appropriate HRP-conjugated secondary antibody (Abcam; ab6721 or ab6789). Finally, bound secondary antibodies were visualized by ECL detection reagent (BioRad) and images were acquired by an imaging system equipped with CCD camera (ChemiDoc, Bio-Rad). Immunoprecipitations for KEAP1 (Santa Cruz Biotechnology; sc-514914) and NRF2 (Abcam; ab137550) were performed on 1000 µg of proteins. Lysates were incubated overnight with Agarose Protein G plus mixture (Pierce) and protein complexes were eluted in Laemmli buffer. Then, Western Blot analysis were performed as described above. Chromatin immunoprecipitation was performed using EpiQuik Tissue Chromatin Immunoprecipitation (ChIP) Kit (EpiGentek) according the manufacturer's instructions. For ChIP, samples were incubated overnight with GATA-4 monoclonal antibody (ThermoFisher; MA5-15532) and Anti-Histone H3 (tri methyl K4) antibody-ChIP grade (Abcam; ab8580). The following primary antibodies were used: NRF2 (Abcam; ab137550), KEAP1 (Santa Cruz Biotechnology; sc-514914), ubiquitin (Abcam; ab7780); p44/42 MAPK (Erk 1/2) (Cell Signaling; 4965S), Phospho-p44/42 MAPK (Erk1/2) (Thr202/Tyr204) (Cell Signaling; 4370S), GATA4 (phospho S105) antibody (Abcam; ab92585), GATA4 antibody (Abcam; ab227512), and β-actin (Abcam; ab179467). Quantification of the signal was assessed using ImageJ software.

Histology

Paraffin-embedded tissue sections of the liver were used for hematoxylin-eosin staining and frozen sections of the liver for Oil Red O staining. The slides were scanned with Panoramic 250 Slide Scanner.

Mouse biochemical parameters

Total triglycerides content was determined using colorimetric techniques using commercially available reagents (Roche; TG 12016648).

Malondialdehyde and reactive oxygen species content measurement.

Malondialdehyde content was measured using a Lipid Peroxidation (MDA) Assay Kit (Colorimetric/Fluorometric) (Abcam; ab118970). Reactive Oxygen Species (ROS+RNS) were determined using OxiSelect In Vitro ROS/RNS Assay Kit (Green Fluorescence) (NordicBiosite). Intracellular ROS were determined using DCFDA / H2DCFDA - Cellular ROS Assay Kit (Abcam; ab113851). Intracellular RNS levels were assessed using Cell Meter™ Fluorimetric Intracellular Nitric Oxide (NO) Activity Assay Kit *Orange Fluorescence Optimized for Microplate Reader (AAT

Bioquest). Extracellular release of H₂O₂ was measured using Amplex™ Red Hydrogen Peroxide/Peroxidase Assay Kit (Life Technologies). All assays were performed following manufacturer's instructions.

Transmission electron microscopy (TEM)

Preparation for transmission electron microscopy (TEM) was performed according to a published protocol (57). For numerical density measurements of mitochondria in the liver, digital images of liver cell cytoplasm were randomly taken at a final magnification of 5000X. Printed digital images were used and the number of mitochondria was calculated by point counting using ImageJ software. 20 sections/mouse were analyzed.

Flow Cytometry

Non-parenchymal cells were stained with the following fluorophore-conjugated primary antibodies and dyes: Viability Dye SYTOX Blue (ThermoFisher Scientific); F4/80-APC (BioRad), CD11b-PE-Cy7 (BD Biosciences), CD45-PE-CF594 (BD Biosciences). Cells were washed two times with FACS buffer (1% BSA in PBS) after staining, and samples were sorted using a BD FACS Aria Fusion.

Bioinformatics

mir-144 promoter in silico analysis. The *mir-144* promoter region was analyzed for GATA4 binding doain using **Cis-element Cluster Finder** (CISTER) software (58).

Retrieving raw sequencing data. Signal intensities were converted to individual base calls during the sequence run using the system's real time analysis (RTA) software. Sample de-multiplexing and conversion to fastq-files was performed using Illumina's bcl2fastq software with all default options. The distribution of reads per sample in a lane was within reasonable tolerance.

mRNA-seq alignment and gene quantification for HFD and ND mice. Raw fastq-files (PRJNA483744) (10) were aligned against the murine genome version mm10 using TopHat version v2.0.13 (59) with all default options. BAM files containing the alignment results were sorted according to the mapping position. mRNA quantification was performed using FeatureCounts from the Subread package (60) against the GRCm38-gencode transcripts database version seven (gencode.vM7.annotation.gtf) and the GRCh38-genocode transcripts database version 24 (gencode.v24.annotation.gtf) to obtain read counts for each individual Ensembl gene.

GRO-seq data processing and gene quantification for HFD and ND mice. Raw fastq-files (PRJNA483744) (10) were aligned against the murine genome version mm10 using BWA (59) with samse option. Uniquely mapped reads were extended to 150bp in the 5' to 3' direction and used for downstream analysis. Nascent transcription of genes was measured using GRO-seq reads mapped to the sense strand of the gene in a 10kb window (+2kb to +12kb relative to transcription start site (TSS)) within the gene symbol annotated gene body. Smaller genes between 2kb and 12kb in length were quantified using smaller window size, from +2kb to the transcription end site (TES). For genes shorter than 2kb, the entire gene body was used for the quantification. The mapped reads within each gene quantification window were counted using bedtools with the intersect option (61) and expressed as reads per kb per million reads (RPKM). Genes with transcription levels greater than 0.3 RPKM were considered as being actively transcribed. Genes that were not transcribed throughout all conditions were eliminated before downstream analysis. A gene was defined as 'differential' between a given pair of conditions if it was transcribed in either condition and the fold-change was greater than 1.5 (either up or down).

Analysis of RNA sequencing data from ob/ob and wt mice. Raw reads were aligned to the mouse genome mm10 (genome build GRCm38.p5) using STAR aligner (62) and followed by expression quantification at gene level based on Gencode M14 annotation using the Cufflinks pipeline (63). Cuffdiff (64) was used to identify genes differentially expressed between ob/ob and wt mice. GO enrichment and pathway over-representation analysis were further performed on differentially expressed genes between conditions (adjusted p-value < 0.05 and log2-scale fold change > 1 or < -1). Raw fastq files and processed data are available in GEO repository (GSE132801, GSE132800).

NRF2 targets. NRF2 target genes (antioxidant, phase 1 and phase 2) were downloaded from the WikiPathways (Pathway:WP2884) (65). Human gene names were converted into mouse orthologues for downstream analysis using Ensembl BioMart version 92.

Analysis of small RNA sequencing data. After removing the adaptors from the raw reads by Cutadapt (66), ShortStack (67) was used to align the small RNA reads against GENCODE mouse primary assembly (release M14, GRCm38.p5) and further identify the miRNA clusters in de-novo mode. ShortStack quantified the expression of the most abundant RNAs (MajorRNA) at locus as reads per million (RPM) but ignored the quantification for less abundant RNAs (MinorRNA) at the same locus. This could result in false negative discovery of certain miRNAs which are truly expressed in the samples but show no expression due to the quantification. Here, post-processing was performed to

quantify the less abundant RNAs by retrieving read counts from the MinorRNA alignments and converted into RPMs. All quantified miRNAs were then annotated into miRBase by aligning the sequences against miRBase mature miRNA sequence database using BLAST (68). All the miRNAs quantified from each sample were then pulled together into an expression matrix for downstream analysis. ANOVA was used to identify miRNAs differentially expressed between conditions based on adjusted pvalue < 0.05 and at least one condition has median RPMs over 2. Raw fastq files and processed data are available in GEO repository (GSE132795).

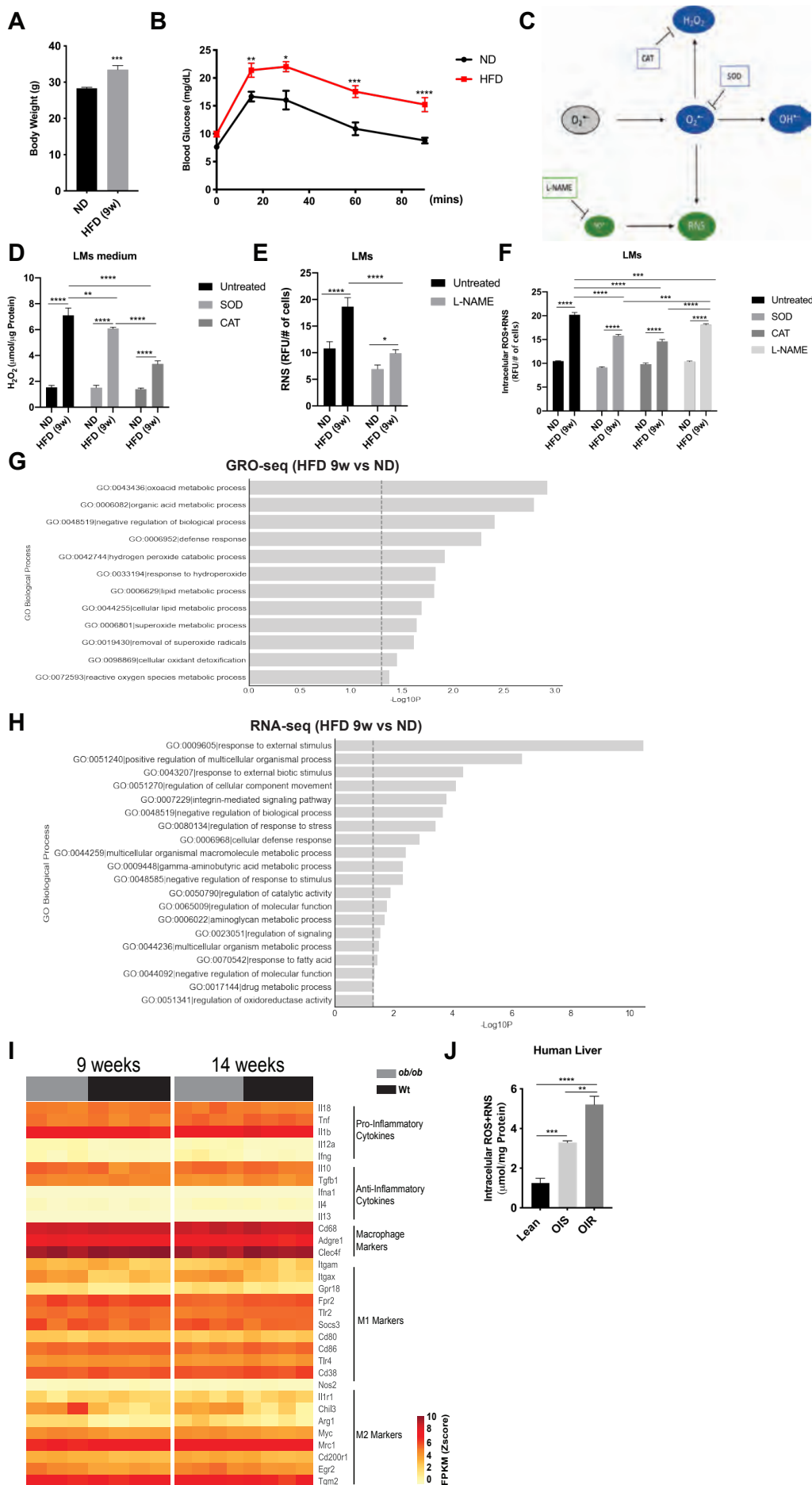


Fig. S1. Oxidative stress in LMs fails to trigger an appropriate antioxidant response in obesity-induced insulin resistance. (A) Body weight of mice fed an HFD or ND for 9 weeks (n=10 per condition). (B) IP-GTT of mice fed an HFD or ND for 9 weeks (n=10 per condition). (C) Schematic representation of inhibitor studies. (D) Extracellular H₂O₂ content in media from LMs of 9 weeks old HFD and ND mice treated with exogenous SOD or CAT (n=3 per condition). (E) Intracellular RNS content in LMs of 9 weeks old HFD and ND mice treated with L-NAME (n=3 per condition). (F) Total intracellular ROS/RNS content in LMs of 9 weeks old HFD and ND mice treated with SOD, CAT or L-NAME (n=3 per condition). (G) Gene Ontology (GO) analysis from GRO-seq dataset comparing mice fed an HFD for 9 weeks with ND. (H) Gene Ontology (GO) analysis from RNA-seq dataset comparing mice fed an HFD for 9 weeks with ND. (I) Expression heatmap of pro-inflammatory cytokines, anti-inflammatory cytokines, macrophage, M1 and M2 marker targets in *ob/ob* mice compared to wt (n=4 wt, n=3 *ob/ob* for 9 weeks; n=4 per condition for 14 weeks). (J) Total intracellular ROS/RNS content in livers from lean, OIS and OIR human individuals (n=5 per condition). Data are mean values \pm SEM. *p<0.05, **p < 0.01, ***p < 0.001, **** p < 0.0001. FPKM, Fragments Per Kilobase Million. See also **table S5-S8**. Related to **Fig. 1**.

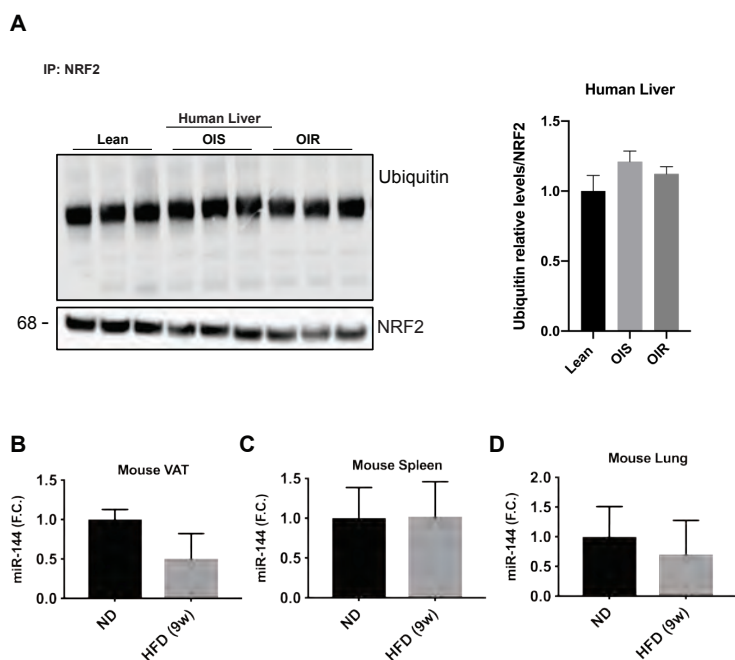


Fig. S2. NRF2 is a target of *miR-144* in obese LMs. (A) WB of ubiquitin and NRF2 after immunoprecipitation of NRF2 from livers isolated from Lean, OIS and OIR human individuals (n=3 per condition). Densitometry representing NRF2 ubiquitination/NRF2 ratio. (B) Stem-loop RT-qPCR analysis of miR-144 performed on Visceral Adipose Tissue (VAT) from HFD and ND-fed mice (n=3 per condition). Data are expressed as fold change (F.C.) compared to ND-fed. (C) Stem-loop RT-qPCR analysis of miR-144 performed on Spleen from HFD and ND-fed mice (n=3 per condition). Data are expressed as fold change (F.C.) compared to ND-fed. (D) Stem-loop RT-qPCR analysis of miR-144 performed on lung samples from HFD and ND-fed mice (n=3 per condition). Data are expressed as fold change (F.C.) compared to ND-fed. Related to **Fig. 2**.

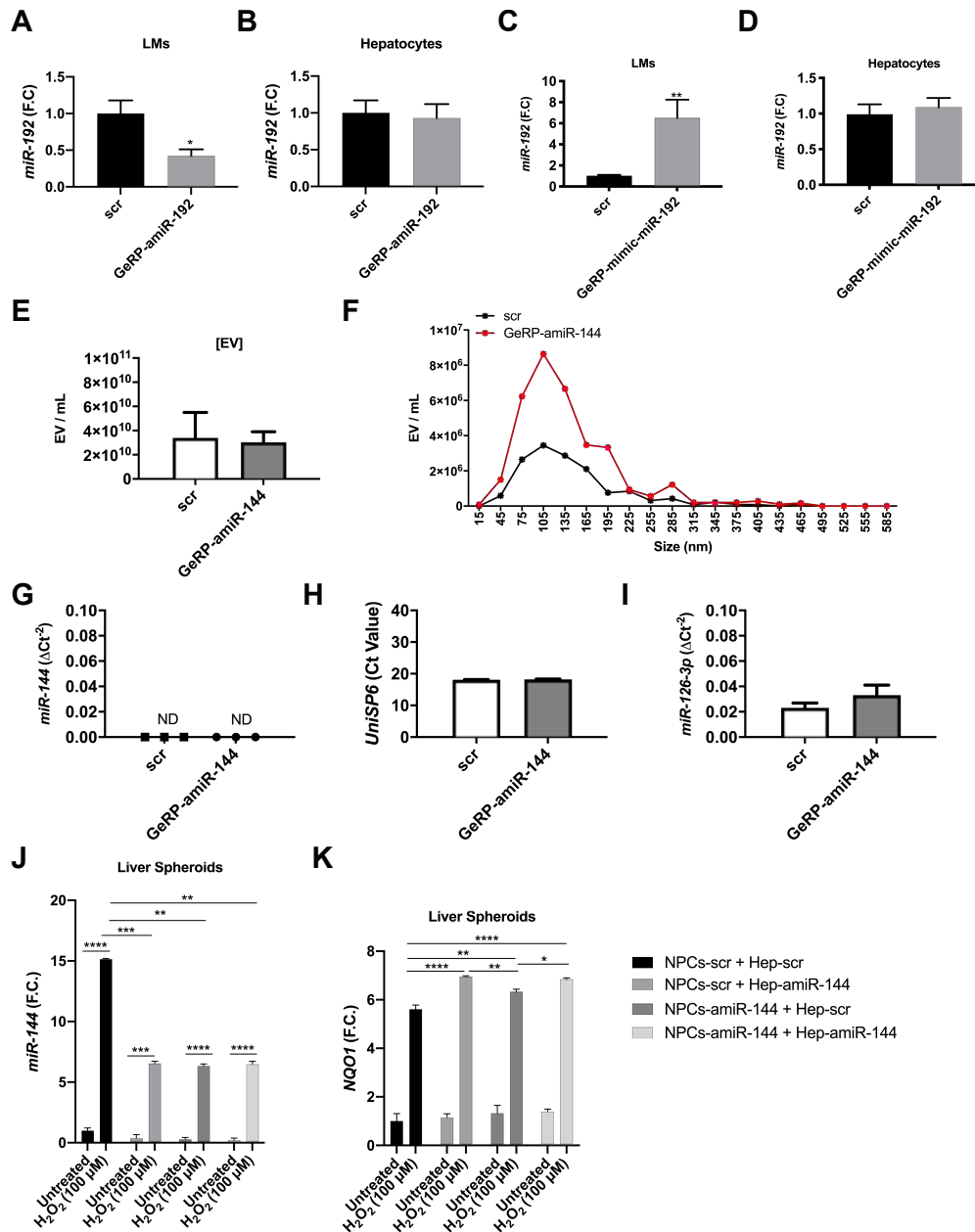


Fig. S3: Silencing miR-144 in LMs reduces ROS release and leads to a decreased expression of miR-144 in hepatocytes. (A) stem-loop RT-qPCR analysis of *miR-192* performed on LMs isolated from scrambled control (scr)- and GeRP-amiR-192 treated mice (n=4 per condition). Data are expressed as fold change (F.C.) compared to scr; (B) stem-loop RT-qPCR analysis of *miR-192* performed on hepatocytes isolated from scr- and GeRP-amiR-192 treated mice (n=4 per condition). Data are expressed as fold change (F.C.) compared to scr; (C) stem-loop RT-qPCR analysis of *miR-192* performed on LMs isolated from scr- and GeRP-mimic-miR-192 treated mice (n=4 per condition). Data are expressed as fold change (F.C.) compared to scr; (D) stem-loop RT-qPCR analysis of *miR-192* performed on hepatocytes isolated from scr- and GeRP-mimic-miR-192 treated mice (n=4 per condition); (E) Concentration of EV isolated from media of LMs isolated from

scrambled and GeRP-amiR-144 treated mice (n=4 per condition); **(F)** EV content in media collected from LMs isolated from scr- and GeRP-amiR-144 treated mice (n=4 per condition); **(G)** stem-loop RT-qPCR analysis for *miR-144* on EV isolated from media of LMs isolated from scr- and GeRP-amiR-144 treated mice (n=4 per condition). ΔCt^2 values; **(H)** stem-loop RT-qPCR analysis for UNISP6 on EV isolated from media of LMs isolated from scr- and GeRP-amiR-144 treated mice (n=4 per condition). Ct values; **(I)** stem-loop RT-qPCR analysis for *miR-126* in EV isolated from media of LMs isolated from scr- and GeRP-amiR-144 treated mice (n=4 per condition). ΔCt^2 values.; **(J)** Stem-loop RT-qPCR analysis of *miR-144* in hepatocytes (Heps) from human liver spheroids untreated or exposed to 100 μM H_2O_2 and treated with scr- and amiR-144 (pooled liver organoids from 3 human donors); **(K)** RT-qPCR analysis of NRF2 target gene *NQO1* hepatocytes (Heps) from human liver spheroids untreated or exposed to 100 μM H_2O_2 and treated with scr- or amiR-144 (pooled liver spheroids from 3 human donors). All qPCR data are fold change (F.C.) compared to scr. Data are mean values \pm SEM. **p < 0.01. Related to **Fig. 4**.

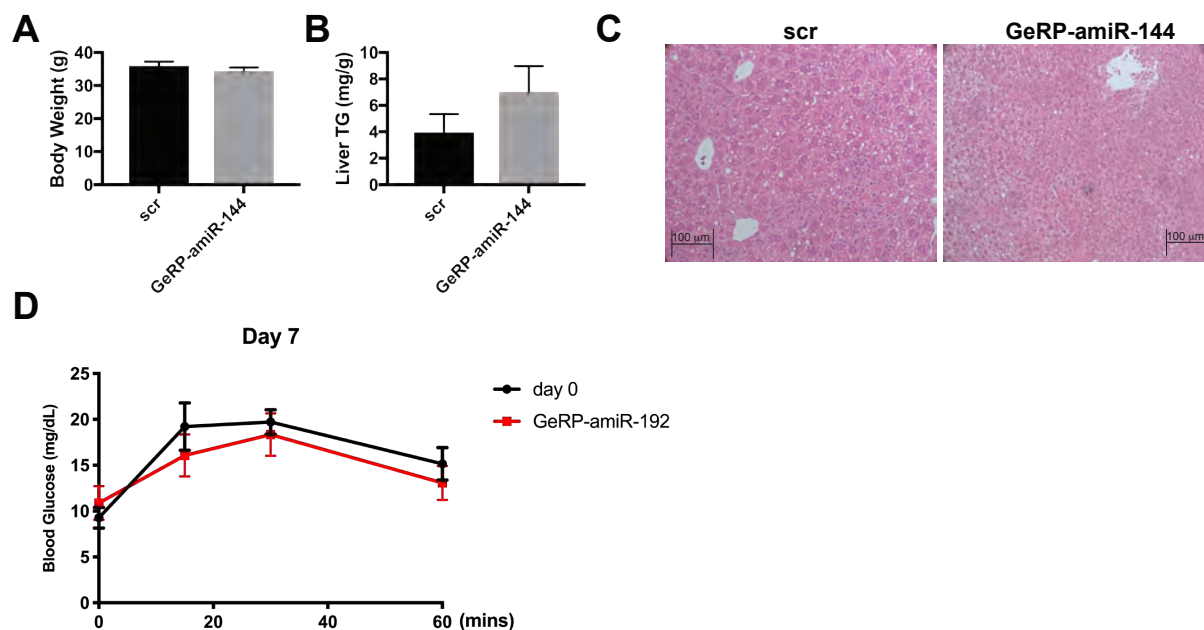


Fig. S4: Silencing *miR-144* in LMs reduces oxidative stress and improves hepatic metabolism in insulin resistance. (A) Body Weight of scrambled and GeRP-amiR-144 treated mice (n=10 per condition) (B) Liver triglycerides content of scrambled and GeRP-amiR-144 treated mice (n=4 per condition); (C) H&E staining of livers from scrambled and GeRP-amiR-144 treated mice (scale bar, 100 μ m); (D) IP-GTT in GeRP-amiR-192 treated mice. Day 0 vs Day7 of treatment. (n=4 per condition). Related to **Fig. 5**.

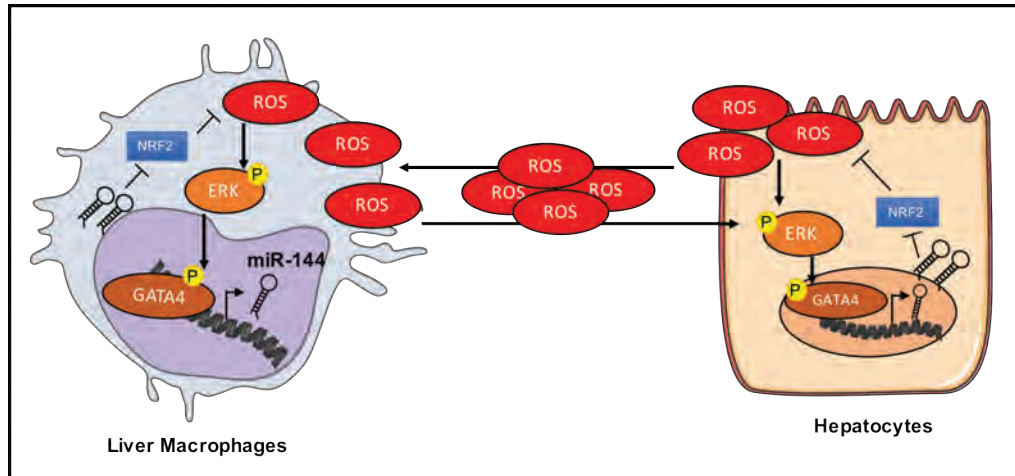


Fig. S5: Proposed model of oxidative stress regulation by LMs in obesity. Excessive lipid accumulation in liver during obesity leads to oxidative stress. LMs exacerbate ROS release without resulting in an overt pro-inflammatory phenotype. ROS, as a secondary messenger, activate ERK and GATA4, increasing expression of NRF2-targeting *miR-144*. The subsequent downregulation of NRF2 protein prevents both cell types to engage an appropriate antioxidant response.

